# Motion and Posture Tracking for Assisted Living

*A dissertation*
*submitted in partial fulfillment of*
*the requirements for the degree of*

**Master of Technology**

*by*

**V. Adithya**
**(10330017)**

*under the supervision of*
**Prof. P. C. Pandey**


Biomedical Engineering Group
Department of Biosciences and Bioengineering
Indian Institute of Technology Bombay
June 2012

# M. Tech. Dissertation Approval

This dissertation entitled **"Motion and Posture Tracking for Assisted Living"** by **V. Adithya** (Roll No. **10330017**) is approved, after the successful completion of *viva voce* examination, for the award of the degree of **Master of Technology** in **Biomedical Engineering.**

**Supervisor** ..... 20/6/2012 (Prof. P. C. Pandey)

**Examiners** ..... (Prof. V. K. Madan)

..... (Prof. V. M. Gadre)

**Chairperson** ..... 20/6/12 (Prof. K. Chatterjee)

Date: 20 June 2012

Place: Mumbai

# Declaration

I declare that this M.Tech dissertation represents my ideas in my words and where ideas or words from others are taken, I have adequately cited and referenced the original sources. I declare that I have adhered to all principles of academic honesty and integrity and have not misrepresented or fabricated or falsified any idea/data/fact/source in my submission. I understand that any violation of the above will be cause for disciplinary action by the Institute and can also evoke penal action from the sources which have thus not been properly cited or from whom proper permission has not been taken when needed.

(V. Adithya)

Date: 20 June 2012

Place: Mumbai

V. Adithya / Prof. P. C. Pandey (Supervisor): “Motion and Posture Tracking for Assisted Living”, *M.Tech. dissertation*, Department of Biosciences and Bioengineering, Indian Institute of Technology Bombay, June 2012.

## ABSTRACT

An inertial measurement system is developed for motion and posture monitoring. The sensing module consists of a triaxial accelerometer, a triaxial gyroscope, a microcontroller, and an on-board serial flash memory, for continuously acquiring and storing the acceleration and angular velocity information for later transfer to a PC. The functioning of the sensors and signal acquisition and storage has been tested using a lab setup.

A software is developed for orientation estimation by fusion of the sensor outputs using offline signal processing. It is implemented using MATLAB and involves an extended Kalman filter for fusing the quaternions computed from the accelerometer outputs and the complementary information provided by the angular velocity measurements. The relative RMS error of the filter output was found to be 6.5%.

# CONTENTS

# List of abbreviations

| Abbreviation | Explantation |
|---|---|
| ADC | analog to digital converter |
| CMG | control moment gyroscope |
| ECP | Educational Control Products |
| EKF | extended Kalman filter |
| FIFO | first in first out |
| $I^2C$ | inter integrated circuit |
| ID | identification |
| IMU | inertial measurement unit |
| I/O | input/output |
| ISR | interrupt service routine |
| MEMS | micro electro mechanical systems |
| OTG | on-the-go compliance |
| PC | personal computer |
| PCB | printed circuit board |
| PLL | phase locked loop |
| QUEST | quaternion estimate |
| RAM | random access memory |
| SPI | serial peripheral interface |
| UART | universal asynchronous receiver/transmitter |
| USB | universal serial bus |

# List of Figures

# List of Tables

# List of symbols

| Symbols | Explanation |
|---|---|
| $x$ | displacement |
| $a$ | acceleration |
| g | acceleration due to gravity |
| $\omega$ | angular velocity |
| $m$ | mass |
| $\psi$ | yaw |
| $\theta$ | pitch |
| $\phi$ | roll |
| $a_{off}$ | accelerometer offset |
| $a_{scale}$ | accelerometer scale factor |
| $g_{off}$ | gyroscope offset |
| $g_{scale}$ | gyroscope scale factor |
| $q$ | quaternion |
| $t$ | time |
| $\mathbf{x}_k$ | state vector |
| $\mathbf{z}_k$ | measurement vector |
| $F_k$ | transition matrix |
| $C$ | measurement matrix |
| $Q_k$ | process noise covariance matrix |
| $R_k$ | measurement noise covariance matrix |
| $P_k$ | error covariance matrix |

# Chapter 1
# INTRODUCTION

## 1.1 Background

Tracking of motion and posture for diagnosis and treatment monitoring purpose is widely done in rehabilitation medicine and assisted living. A number of motion tracking techniques using optical, acoustic and inertial/magnetic tracking systems are used for this purpose. Optical tracking systems sense light patterns and use this information to detect motion [1], [2]. Image based systems use multiple cameras to track pre-designated points on a moving object within a working volume [3], [4]. Acoustic tracking systems use time-of-flight and triangulation or phase-coherence to determine position [5]. Motion tracking using inertial and magnetic sensors is gaining popularity because it does not suffer from range limitations and interference problems faced by the techniques using excitation sources [6]–[9]. This kind of inertial measurement unit (IMU) usually comprises of accelerometers for sensing translational accelerations, gyroscopes for detecting angular velocities and sometimes a magnetometer for directional data. These sensors are low cost and they are available in compact sizes [6]–[17].

Small sized body wearable IMUs are used for tracking posture and motion in medical applications by using single or multiple sensor units attached to various parts of the body, usually the trunk, wrists, and ankles. The orientation and position of these sensors could be found with respect to each other, or with respect to an earth fixed reference frame [6]–[18].

Home-based intelligent monitoring systems for rehabilitation and assisted living for providing both therapeutic instruction and support information are well recognized [18]–[22]. These systems measure various parameters using inertial sensors that correspond to the limb movements made by the participant and the information would be fed back to the person in audio or visual format and also, when necessary, to their health care professionals. For stroke rehabilitation, the motion trajectory and the velocity of the forearms are used as parameters to understand the

effects of arm training on muscle properties [18]. For fall analysis in elderly persons, displacement of the toe from the ground during walking and the velocity of walking were measured by Lai *et al*. [23] and the trunk position was monitored by Huang *et al*. [24]. In amputee rehabilitation, Churko *et al*. [25] used an IMU for tracing the 3-D trajectory of the prosthetic arm worn by the patient and it was given as an input to the intelligent rehabilitation system. Lorussi *et al*. [26] and El-Gohary *et al*. [27] measured joint angles as parameters to estimate mobility in patients with neurological disorders and for injury rehabilitation. Leg and hand movements, measured using inertial sensors were used to quantify sleep quality and duration in patients suffering from insomnia [28]–[30].

## 1.2 Project objective

The parameters for posture tracking are the three angles: roll (the angle about the x-axis), pitch (the angle about the y-axis), and yaw (the angle about the z-axis). The parameters for motion tracking are the angular velocity, linear acceleration, linear velocity, and the displacement which is also called the motion trajectory. The project objective is to develop an IMU for motion and posture tracking for people in assisted living facilities and rehabilitation centers. The acceleration in the X, Y and Z directions are measured using a triaxial accelerometer and the angular velocities about the three directions are measured using a triaxial gyroscope, and the data are acquired and stored using a microcontroller in an onboard serial flash. The data stored in the serial flash can be transferred to a PC for processing using a quaternion based extended Kalman filter and displaying posture and motion related information.

## 1.3 Report outline

The second chapter provides an overview of the motion and posture tracking techniques. The IMU hardware is described in the third chapter. Chapter 4 describes the IMU software. The testing of the unit is presented in the fifth chapter. Chapter six presents the quaternion based extended Kalman filter algorithm for orientation estimation. The last chapter provides a summary of the work completed and suggestions for future development.

# Chapter 2

# MOTION AND POSTURE TRACKING TECHNIQUES

## 2.1 Introduction

This chapter provides a review of the applications of motion and posture tracking for assisted living, rehabilitation assist devices for stroke and other neurological disorders like Parkinson's disease, amputee and prosthetic rehabilitation aids, and sleep disorder monitors. This is followed by a description of various inertial sensors available and the algorithms used for motion and posture tracking.

## 2.2 Application of motion and posture tracking

Fall is a major source of morbidity and mortality among the elderly [23], [24], [31]. Fall detectors worn on the waist record the trunk position throughout the day [24], [31]. A fall is classified based on the initial and final positions of the trunk during fall and the occurrence of the fall is identified by the rate of change of position of the trunk. Two types of inertial sensors can be used for this: triaxial accelerometer [31] and biaxial gyroscope [24]. When using the triaxial accelerometer for front or side-ways fall detection, two end points when the accelerometer value goes above a particular threshold and returns back are identified and time stamped. The positions at these points are identified from the orientation of the sensor and a fall is classified. When using a biaxial gyroscope, the angular velocity used to identify a fall and position is derived by integrating angular velocity. Another method described in [23] analyzes tripping and slipping falls by measuring the displacement of the foot from the ground and velocity of walking using a triaxial accelerometer and biaxial gyroscope. Here the biaxial gyroscope is used only for identifying the swing cycle. The activities of daily living [32] like walking and climbing are used as a measure of mobility and also for monitoring exercise cycles. A triaxial accelerometer, gyroscope and magnetometer would provide the required displacement, velocity and orientation information.

Stroke is a condition when the blood supply to a part of the brain is absent due a blockage in the artery or due to hemorrhage (leakage of blood) [33]. This adversely affects the brain function and can result in an inability to move one or more limbs on one side of the body. Rehabilitation for patients who have suffered a stroke is important to recover movements in the limbs paralyzed by stroke. It involves exercises monitored by a trained professional and periodic assessment of the effectiveness of the exercises [34]. A home based rehabilitation system [18], [37] has an audio and visual interface that has many exercise modules; it also has a sensor interface that monitors the actual limb movement. These movements are analyzed by the system and a feedback is provided. This information can also be sent to the professionals. The common motion capturing methods used for this application are the visual [3], [4] and optical based tracking systems [1], [2]. Zhou *et al.* [18] and Ahmed *et al.* [34] reported inertial sensor based tracking systems using triaxial accelerometer, gyroscope and magnetometer. This application requires tracking the joint angle movements, extent of flexion and extension of joints and various other gestures movements.

Parkinson's is a neurodegenerative disease which results in loss of limb mobility and tremors [33]. Other neurodegenerative diseases are Alzheimer's, and Huntington's. Movement symmetry is one important index for the identification and evaluation of Parkinson's; another is tremor analysis during rest. Lorussi *et al*. [26] and Anna *et al*. [36] used multiple sensors on the body. Normally only gyroscopes or gyroscopes and accelerometers are used.

Actigraphy is a technique for quantifying sleep using an accelerometer and light sensors [37]. The assumption here is that there is very small body movement during sleep and the movement significantly increases when awake. Methods used for sleep quantification are generally based on thresholding [38]–[40]. The downside of this method is that restless movement of the limb (e.g., periodic leg movement) during sleep could be classified as activity and minimal activity during extended periods of nocturnal wakefulness tends to get classified as rest [37]. It was however observed that these factors tend to be consistent from night to night in insomnia patients, so actigraphy may be useful in the assessment of sleep variability or in the measurement of treatment effects. Gorny *et al*. [41] provided evidence that the wrist activity pattern in delayed sleep phase syndrome recorded for a few days proved to be a very good

measure in analyzing the effect of certain drug. Actigraphy has also been used to assess sleep patterns in young [42]. Children and babies move significantly when awake and are quite still when asleep. Actigraphy was used in a study to compare sleep patterns of HIV-infected children and normal children and significant correlation has been reported between actigraph data and subjective reports for night waking. Actigraphy has also been used for studying sleep patterns of newborns with respect to gestational age, and for monitoring the effect of melatonin administration on sleep continuity in children with germ cell tumor involving the pineal region [42]. The use of triaxial accelerometer and gyroscope for actigraphy is still unexplored. Using more than one module of these sensors attached to various parts of the body is bound to give more accurate results. Also specific conditions like restless leg syndrome can be more accurately identified.

A sensor module, more widely called an inertial measurement unit (IMU) having a triaxial accelerometer and a triaxial gyroscope would give sufficient results for most of the above applications. It would be helpful in tracking position in a two-dimensional plane and measurement acceleration and angular velocity in all the three directions.

## 2.3 Sensors

### *2.3.1 Accelerometer*

An accelerometer is a sensor that gives a voltage output proportional to the acceleration of the body to which the sensor is attached. In its basic form, it has an inertial frame to which a fixed mass is connected by a spring [43]–[46]. This setup can measure the acceleration along the axis of the spring. Let the frame is subjected to a constant acceleration *a*. At steady state, the mass *m* which is at rest relative to the frame will also have an absolute acceleration of *a*, and hence will experience a force equal to *ma*. As the mass is not in motion relative to the frame, a force is developed across the spring causing a displacement *x* between its two ends, and it is given as,

$$x = ma/k \tag{2.1}$$

where *k* is the spring constant. This displacement is converted into voltage by a strain or displacement sensor. The acceleration sensed by the accelerometer is thus a measurement of the force acting on the mass *m* along the axis of the spring. This also includes the gravitational force, and hence an accelerometer cannot distinguish

between a force produced because of the acceleration of the sensor frame and the component of the gravitational field along the spring. The MEMS accelerometer has beams attached to a central mass, these beams move between fixed beams causing a voltage to be produced proportional to the acceleration [45], [47]. Some available MEMS sensors include BMA180 from Bosh [48], MMA series from Freescale Semiconductors [49], and LIS3LV02DQ from STMicroelectronics [50].

*2.3.2 Gyroscope*

A gyroscope is a sensor that gives a voltage output proportional to the angular velocity of the body the sensor is attached to. It works on the principle of Coriolis effect [1]. When a body with mass *m* moves with a constant velocity *v*, in a reference frame which is rotating at an angular velocity $w$, the body experiences a Coriolis force in the direction perpendicular to its velocity, the magnitude of the force is given by

$$F = -2mwv\sin\theta \tag{2.2}$$

where $\theta$ is the angle between the direction of movement of the body and the axis of rotation. The MEMS gyroscope has a vibrating crystal or vibrating silicon ring that acts as the body moving with constant velocity. During the rotation of the sensor, the Coriolis force acting on the crystal or silicon ring changes its direction of vibration which is sensed by a capacitive sensor and a voltage output proportional to the angular velocity is generated. Some of the MEMS gyroscopes available in the market are L3G4200D from STMicroelectronics [51], IMU3000A from Invensense [52], and ADXRS450 from Analog Devices [53].

*2.3.3 Magnetometer*

A magnetometer is a device that measures the magnetic field in the vicinity of the sensor [54]–[55]. In the absence of stronger magnetic fields, it senses the earth's magnetic field. The earth's magnetic field varies spatially due to inhomogeneity of rocks and the interaction between charged particles from the sun and the magnetosphere. Its value is lowest near the equator and increases when moved towards the poles. Simple MEMS based magnetometer works on the Lorentz force principle. A silicon structure on which an excitation coil is deposited is suspended over a glass substrate by torsional beams. The glass substrate has silver deposits that form capacitors with the structure. When a sinusoidal current ($I_0 \sin 2\pi ft$) flows in the

excitation coil, in the presence of a constant magnetic field $B$ parallel to the surface of the structure, the structure experiences a Lorentz force $F_L$ acting on it. Due to the shape of the coil, the force acting on the two sides of the structure separated by the torsional beam is perpendicular to the surface of the structure and opposite in direction. This causes the structure to vibrate. If its frequency of vibration is equal to the frequency of the current, resonance occurs. The magnitude of vibration depends on the strength of the magnetic field, this is sensed by the capacitive structures and a proportional voltage output is given.

$$F_L = I_0 L_C B \sin 2\pi ft \tag{2.3}$$

where $L_C$ is the length of the coil. One of the magnetometers available in the market is HMC6343 three-axis compass from Honeywell [56], mostly magnetometers are available as part of an IMU comprising of all the three sensors, e.g. MAG3 IMU series form Omni Instruments [57], and ADIS16405 from Analog Devices [58].

*2.3.4 Sensor fusion*

An accelerometer senses the sum of the inertial and gravitational force along its axis. A triaxial MEMS accelerometer can be used for sensing the three components of the acceleration along the x, y, and z directions of the sensor module. The three outputs can be used for sensing the magnitude of the net force on the sensor but the direction of these forces can be determined only if orientation of the sensors can be determined. This poses a problem in case of a body worn IMU, because orientation of the sensors changes with the movement of the body part to which the sensor is attached. To eliminate the gravitational force, we need to know the sensor orientation using another sensor. A triaxial gyroscope which gives angular velocity which can in turn be integrated to find the orientation angles can be used for this purpose.

Both accelerometer and gyroscope have measurement errors due to sensor bias and a wideband noise [6]. Bias may be due to the error in sensor alignment on the board or internal misalignment. The wideband noise may be caused by the thermal noises, or vibration of the body the sensor is attached to. Even if the bias error is compensated, bias instability can change it slowly over time. The bias and the bias instability cause drift in the angle and linear velocity measurement obtained by integrating the angular velocity data from the gyroscope and the acceleration data

from the accelerometer. This problem can be solved by fusing the output of the two sensors using a fusion algorithm.

## 2.4 Orientation estimation methods

Several sensor fusion algorithms have been reported to estimate relative orientation of two or more sensors with respect to each other or their orientation relative to an earth-fixed reference frame. Two or three degrees of orientation in a plane are estimated based on the type, number, and configuration of sensors used.

Lee and Ha [10] designed a motion tracking system, based on linear accelerometers to sense the angular movements at a joint with two degrees of freedom. For slow movements, a triaxial accelerometer was used to determine the joint angles. For fast movements, data from two sets of triaxial accelerometer units were combined using geometric sensor fusion technique to separate gravitational acceleration from motion-related linear acceleration.

Gebre-Egziabher *et al*. [11] described an algorithm for estimation of the orientation of a rigid body for aircraft applications. Magnetometer and accelerometer measurements were used to calculate the quaternion using a Kalman filter, without the use of angular rate sensors. The algorithm was applicable for stationary or slow moving applications, and not for highly dynamic tracking applications.

Chin-Woo *et al*. [12] proposed a gyroscope-free inertial navigation system that used six accelerometers to determine both linear and angular motions of a rigid body. They have described an algorithm that tested for a sufficient condition to determine acceptable configuration of the accelerometers. The linear and angular motion for this configuration was computed separately using two decoupled equations of an input-output dynamical system. Use of accelerometers to calculate angular rate resulted in a faster orientation error growth rate than that associated with gyroscopes. This is due to inclusion of the angular acceleration terms which introduce drift due to integration.

Rehbinder and Hu [59] have described an attitude estimation algorithm using data from a triaxial gyroscope and a triaxial accelerometer. They estimated the Euler angles roll and pitch using a Kalman filter for walking robot application with a switching architecture for slow and fast accelerations. The algorithm was tested only for simulated signal.

Sabatini *et al*. [13] used a sensor module containing a biaxial accelerometer and a gyroscope to perform gait analysis and measurement. The cyclic nature of the human gait was exploited to measure inclination, distance, and speed. Transition from one gait phase to the next was determined from the pitch angle derived from the gyroscope data. Acceleration data was double integrated during the swing phase when the foot leaves the ground and placed forward to determine its position with respect to the vertical when the foot is flat on the ground. The drift in position estimation is reduced by integrating only during the gait phase which is determined from the gyroscope. All motion is assumed to take place in a non-rotating sagittal plane.

Gallagher *et al*. [7] designed a system with three sensor modules, placed on the wrist, upper arm and chest, for real-time body posture tracking for long term monitoring of patients and elderly subjects or for use in biomechanic research. Each sensor module had nine sensors: three orthogonal gyroscopes, accelerometers and magnetometers. The posture tracking algorithm described estimates the roll, pitch and yaw angle from a single sensor data with respect to the earth fixed coordinates, using complementary filters. The technique was validated by comparing the posture output from a robotic manipulator. For brushing and running activities, the coefficient of determination $R^2$ was reported as 0.873 and 0.706, respectively.

Bachmann *et al*. [6], [14]–[16] proposed a quaternion-based extended Kalman filter (EKF) algorithm for human body tracking. A first-order linear system for modeling human body limb motions was proposed in [14]. A Gauss-Newton iteration method was used to preprocess accelerometer and magnetometer data to produce quaternion input to the EKF. Formulation and simulation testing of a reduced-order implementation of the Gauss-Newton iteration method for this Kalman filter was presented in [15]. In [16] and [6] factored quaternion algorithm and QUEST (quaternion estimate) algorithm were used to calculate the quaternion using the accelerometer and magnetometer data. The maximum error was $9^{\circ}$ as observed for signals obtained from the sensor when placed on a Haas precision tilt table. All the processing was done in the PC.

Roetenberg *et al*. [17] used a sensor module with triaxial accelerometer, gyroscope and magnetometer. An extended Kalman filter algorithm which included a magnetometer model designed to prevent heading drift and compensate for magnetic disturbances was used. This compensation allowed a significant improvement in the

estimation accuracy, as compared to the estimation with no compensation or using angular rate sensors only.

Zhu and Zhou [9] used a linear Kalman filtering to smooth accelerometer and magnetometer readings from a sensor module with a triaxial accelerometer, gyroscope and magnetometer. Rather than estimating individual limb segment orientations relative to a fixed reference frame, the system determined the joint angles in axis/angle form using the data from the four sensors. Three sensors were mounted on the body and a fourth sensor was mounted on the wall the body faces, to act as reference. The axis/angle pairs were determined analytically.

Kraft [60] used a quaternion-based unscented Kalman filter for real-time estimation of rigid-body orientation from measurements of triaxial accelerometer, gyroscope, and magnetometer sensors. The linearization of the state equation was done using a set of sample points from the Gaussian probability distribution.

## 2.5 Summary

A review of the methods shows that they mainly differ in terms of accuracy and computational complexity. A larger number of sensors generally results in a better estimation accuracy. With only accelerometers, roll and pitch angle can be calculated when the sensor is stationary. The calculated values do not suffer from drifts and the baseline is maintained even when the accelerometer is in motion. With both accelerometers and gyroscopes, the drifts from the integration of gyroscope data for roll and pitch angles is reduced by comparing the baseline with estimates from accelerometer data using fusion algorithms like complementary filtering or Kalman filtering but the yaw angle estimation is not accurate and suffers from drift errors. With additional magnetometers to obtain the baseline for yaw angle, best estimates for all three angles could be obtained. Hence the application becomes a crucial factor in the selection of the hardware and algorithm.

Complementary filters have estimation bias [61]. A few degrees error causes significant deviation in the linear motion estimation. For a generalized sensor module that could be used for a variety of applications, accelerometer based quaternion estimation for roll and pitch angle with extended Kalman filter would be the logical choice. In the absence of magnetometer, the extended Kalman filter presented in [6] could be modified and used.

For reducing drifts in the integration, smaller integration duration with periodic resetting can be used. To avoid uncertainty of the contribution of the input variable near the edges of the integration interval, we can use overlapping integration intervals. The interval size is determined based on the application a value of 1 s with 0.5 s overlap would provide sufficient approximation for low velocity applications like monitoring of the posture and movement of parts of human body. Another method is the drift subtraction method for applications with cyclic movements. In cyclic movements like walking, arm swinging, continuous flexion-extension of arm, the initial and final velocity in a cycle can be taken as zero, using these two points, the drift can be estimated and subtracted.

# Chapter 3

# INERTIAL MEASUREMENT UNIT HARDWARE

## 3.1 Introduction

This chapter provides a description of the hardware of the inertial measurement unit (IMU). It consists of inertial sensors, namely, accelerometer for measuring linear acceleration and gyroscope for measuring angular velocity. Inertial sensors do not require any external reference as opposed to infrared, radar, or video motion-sensing technologies; also they are not affected by limitation in working conditions such as friction, wind, directions, or dimensions [62]. However, these sensors are prone to intrinsic drift, circuit thermal noise, time discretization and quantization error, vibration and friction noise, etc., apart from offset and sensitivity errors. Error compensation is generally carried out by software, but some sensors have provision for internal correction of offset.

The board has been designed for motion tracking application. A block diagram of the board is shown in Figure 3.1. It consists of a triaxial digital gyroscope, IMU3000A (Invensense) and a triaxial digital accelerometer, MMA8451Q (Freescale Semiconductors), interfaced with 44-pin PIC24F64GB004 (Microchip Technology) as the host microcontroller. Both the sensors are interfaced to the microcontroller using $I^2C$. A 64-Mb serial dual I/O flash SST25VF064C (Microchip Technology) is interfaced to the microcontroller for storing the data. The memory can be used for recording the sensor signals acquired at 100 Hz for two hours. The board has a serial port and an USB for transfer of the stored data to an external device or PC. The board design may later be modified to have magnetometers, and temperature and pressure sensors to further extend the range of its applications.

## 3.2 Sensors

The sensors MMA8451Q and IMU3000A have been chosen for their compact size,

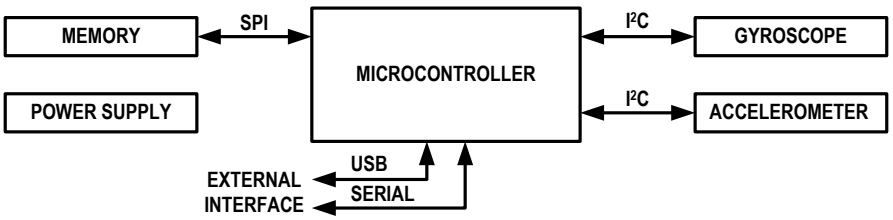


**Fig 3.1** Block diagram of the Inertial Measurement Unit

their inbuilt signal processing functions and their low power consumption. The relevant features of each of the sensors are briefly described below.

MMA8451Q [49] is a low-power, triaxial, capacitive micromachined accelerometer with 14-bit resolution. It has dynamically selectable full-scales of ±2 g, ±4 g, and ±8 g and has a selectable signal sampling frequency of 1.56 Hz–800 Hz. The digital output interface is by $I^2C$ and can operate up to 2.25 MHz with a 4.7 kΩ pull-up. It has two programmable interrupt pins for seven interrupt sources and on-chip 14-bit ADCs. It has an on-chip 32 sample FIFO which allows burst read and internal high-pass filtering with settable cut-off frequency. It operates at 1.95–3.6 V supply with a maximum current of 1 mA. It is compatible with 1.6–3.6 V interface levels.

IMU3000A [52] is a triaxial digital gyroscope with programmable full-scale ranges of ±250/±500/±1000/±2000 °/s and it can withstand up to 10,000 g shock in operation. Its on-chip FIFO and dedicated $I^2C$-master accelerometer sensor bus simplify system timing and lower system power consumption. The sensor bus allows the device to directly acquire data from an off-chip accelerometer without intervention from an external processor. The FIFO allows a system microcontroller to burst read the sensor data. Other features include on-chip 16-bit ADCs, programmable digital filters, a precision clock, an embedded temperature sensor, and programmable interrupts. It can be used for a true 6-axis motion sensing by connecting it directly as a master device to a third-party triaxial digital accelerometer as a slave and clocked from the internal phase locked loop of the master, providing highly accurate timing. It has a supply range of 2.1–3.6 V and consumes a maximum current of 6.1 mA. It is compatible with 1.71–3.6 V interface levels.

Interfacing of the gyroscope U4 and the accelerometer U5 with the microcontroller U1 is shown in Figure 3.2. The $I^2C$ protocol requires two lines:

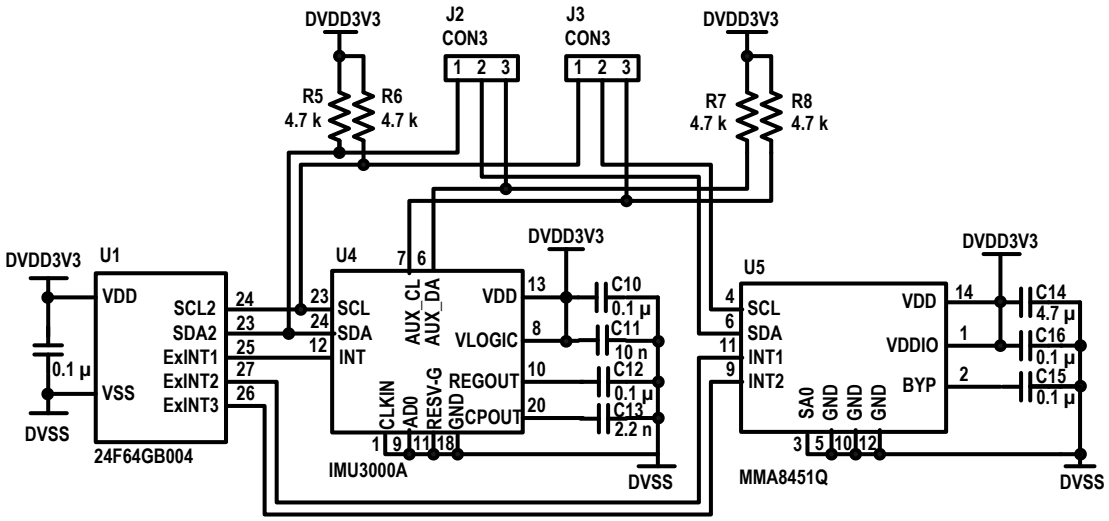


**Fig 3.2** Interfacing of the sensors with the microcontroller

bidirectional data transmission and clock. Both lines require pull-up resistors, preferably 4.7 kΩ. For interfacing to the two sensors, the $I^2C$ module-2 of the host controller has been used. As mentioned previously, the gyroscope has two $I^2C$ modules, the primary module to connect to the host controller and the secondary module to connect to an auxiliary accelerometer. The board is designed to connect the accelerometer to the secondary $I^2C$ module of the gyroscope or to the primary module. In the second case, the host controller can access the accelerometer directly. The type of connection can be selected using jumpers J2 and J3. The accelerometer can be connected directly to the microcontroller by shorting pins 1 and 2 of J2 and also of J3. Alternatively, it can be connected to the secondary $I^2C$ pins 6 and 7 of the gyroscope by shorting pins 2 and 3 of J2 and also of J3. Pull-up resistors have been provided for both the connections. The interrupts of both the sensors have also been connected to the external interrupt pins of the host controller.

## 3.3 Microcontroller, memory and data transfer

At the core of the board is the microcontroller U1 for handling the control and signal acquisition operations. The 44-pin microcontroller PIC24F64GB004 [63] is a 16-bit controller with two SPI, two $I^2C$, and two URAT modules and one USB channel

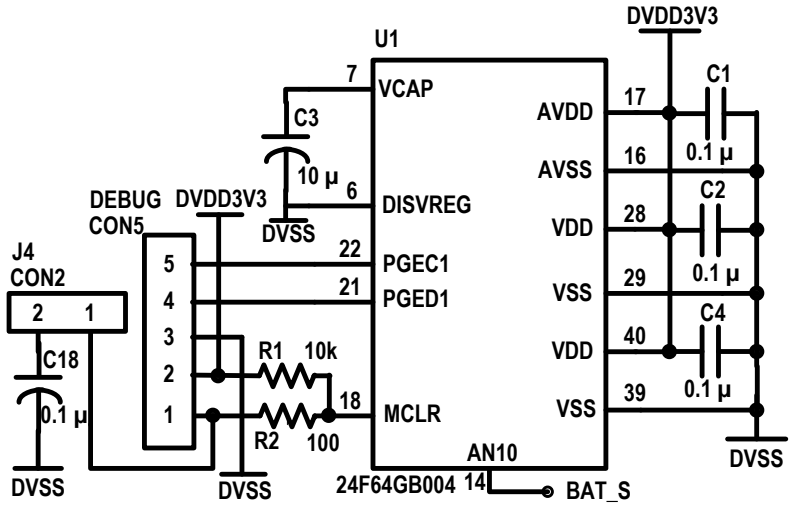


**Fig 3.3** Power supply and debug connections of the microcontroller

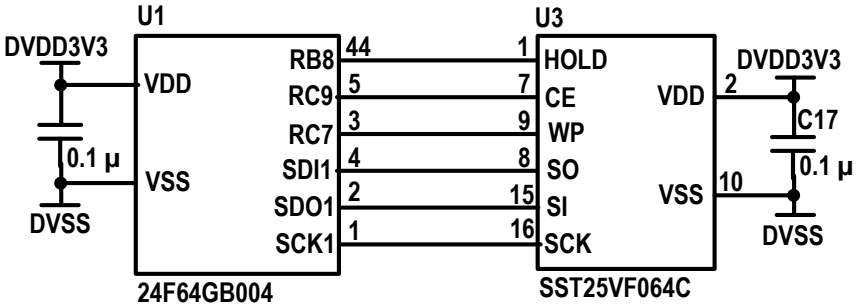


**Fig 3.4** Memory interface

which is "on-the-go (OTG)" compliant. It has an 8 MB RAM and 35 I/O pins. In our application, it is used with a clock source of 96 MHz PLL for a $f_{CY}$ of 4 MHz. It acts as the master in the sensor interfacing using $I^2C$ and the serial flash interfacing using SPI. For data transfer to a PC or other external devices, RS 232 and USB ports can be used. It operates at 2–3.6 V and consumes a maximum current of 25 mA.

The microcontroller has three $V_{DD}/V_{SS}$ and $AV_{DD}/AV_{SS}$ pairs. A 0.1 µF ceramic capacitor has been used as decoupling capacitors between each pair for bypassing noises in the range of 200 MHz, as recommended. The $\overline{MCLR}$ pin provides two device functions: device reset, and device programming and debugging. For attaining the specific voltage levels $V_{IH}$ and $V_{IL}$ and to allow for fast signal transactions, two resistors (R1 and R2) and a capacitor (C18) are connected to the pin as shown in Figure 3.3. The capacitor is to be isolated during programming and

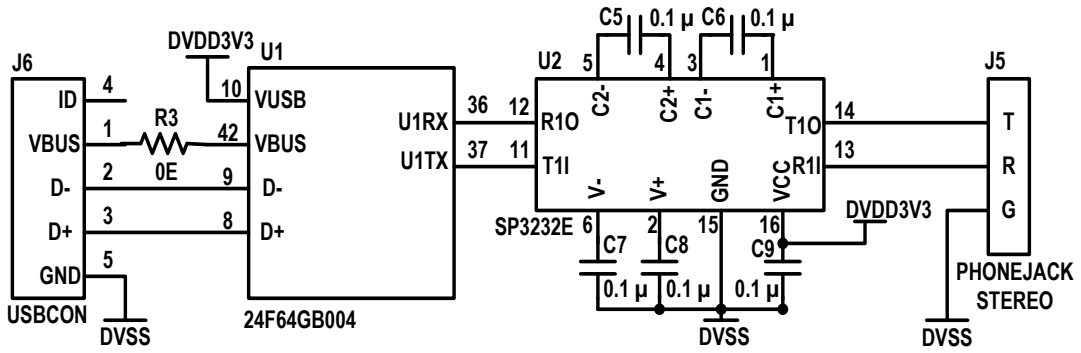


**Fig 3.5** Serial transmission

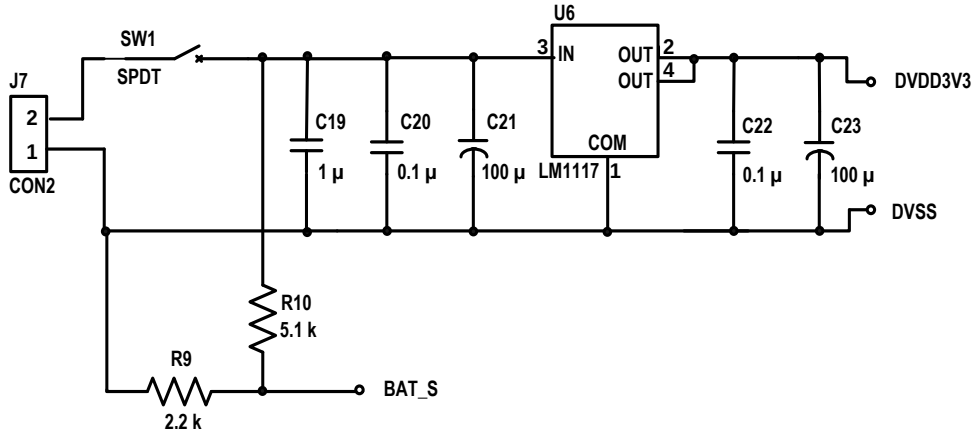


**Fig 3.6** The power supply circuit

debugging operations by disconnecting the jumper J4. The internal regulator enables the device to run its core logic from $V_{DD}$ at an optimal 2.5 V, and it is enabled by connecting the DISVREG pin to $DV_{SS}$ and by connecting a 10 µF to $V_{CAP}$ to maintain regulator stability.

For storing the acquired signals, a 64-Mb serial dual I/O flash memory chip U3 has been used as shown in Figure 3.4. SST25VF064C [64] has a maximum clock frequency of 80 MHz and a page size of 256. It has flexible erase options of 32 Kbyte or 64 Kbyte overlay blocks. Other features include end-of-write detection, write protection, software write protection and security ID. We have six sensor outputs, each with 16-bit resolution. With a sampling frequency of 100 Hz, data can be stored continuously on this chip for nearly 1 hr 57 minutes. It operates at 2.7–3.6 V and has a maximum current consumption of 10 mA. The SPI connection, as shown in the figure, for interfacing the serial flash to the microcontroller requires a minimum of four lines:

one data input, one data output, clock and chip select. In addition, connections have been given for hold and write protect pins.

The data stored in the serial flash can be transferred to an external device or a PC. This transfer can be carried out using either USB or RS232. The microcontroller pin voltage levels are made compatible to RS232 levels (±5 V) by using the driver U2: SP3232 (Sipex) [65]. The transmitter (pin RP20) and receiver (pin RP19) of the microcontroller are used for RS 232 (Figure 3.5). It has two drivers and two receivers and can operate at a maximum data rate of 235 kbps. It operates at 3–5.5 V and consumes a maximum current of 2 mA.

## 3.4 Power supply

It has been decided to operate the microcontroller, the two sensors, RS232 driver, and the serial flash at 3.3 V. As there are no analog components on the board, a single supply can be used to power all the components. The maximum estimated current consumption by the components on the board is 45 mA. We have used a fixed voltage linear low dropout regulator LM1117 (National Semiconductor) [66] for powering the board. It can operate at a minimum dropout voltage of 1.2 V and a maximum output current of 800 mA. Its input voltage range is 4.5–20 V. The maximum power dissipation capacity $P_D$(max) of the regulator is 600 mW.

$$I_L < I_{MAX} \tag{3.1}$$

$$(V_{In\ MAX} - V_{Out}) I_L < P_D \tag{3.2}$$

Let $I_L = 100$ mA

$$V_{In\ MAX} = \frac{P_D}{I_L} + V_{Out} = \frac{600 \times 10^{-3}}{100 \times 10^{-3}} + 3.3 = 9.3 \text{ V} \tag{3.3}$$

Thus taking the load current as 100 mA, the regulator can be operated with 4.5–9.3 V input, without using a heat sink. Hence the input voltage to the regulator can be powered by 6 V PCB mount nickel metal hydride battery with a current capacity of 300 mAh. The resistors R9 and R10 form a voltage divider that gives 0.3 times the regulator input voltage as an input to the ADC for monitoring the input voltage to the regulator as shown in Figure 3.6.

## 3.5 PCB Design

The placement of the sensors on the PCB is very important as they are highly sensitive to noises. The 44-pin microcontroller allows the placement of each of the modules on one side. Both the sensors have been placed on the same side of the controller with the respective axes parallel to each other. All the components are surface mount devices have been placed on the same side of the PCB. The SPI and the UART modules can be configured on any of the 25 remappable peripheral (RPx) pins, allowing a convenient placement of the modules on the PCB.

# Chapter 4

# INERTIAL MEASUREMENT UNIT SOFTWARE

## 4.1 Introduction

This chapter gives a description of the microcontroller program for data acquisition, storage, and transfer. The code is written in C and is divided into two parts: the main program and the interrupt service routine. The main program starts by setting the system clock, initializing the I/O ports pins, initializing the communication modules required to interact with the sensors, serial flash, and PC, configuring the sensors, serial flash, timer and UART interrupts and finally turning on the sensors and enabling the interrupts. Once the initialization is done the controller has no function till either of the interrupt occurs and so it is put in sleep mode during the idle period to save power. In the timer interrupt service routine (ISR) the data is read from the sensors and stored in flash. UART is used for controlling the IMU via the PC and transferring the data from the flash to the PC. The serial flash memory is erased during initialization and gyroscope and accelerometer segment flash address is set to 0x000000 and 0x400001 respectively. Figure 4.1 shows the flow of the main program.

## 4.2 Initialization

The system clock is set at 4 MHz which is the lowest frequency and sufficient for the operation without increasing the power consumption. All I/O pins are set as digital pins. Before the ports pins are configured for the I/O functions, remappable pins (RPx) RP24, RP22 and RP9 are configured as data input, data output and clock pin for SPI for serial flash connection and RP19 and RP20 are configured as receiver and transmitter pin for UART. The other pins of the serial flash, namely, the chip select, write protect and hold are controller by the I/O pins. The SPI module is configured to operate at 4 MHz and it transfers 6 bytes of data at a time from the sensors to the flash. The UART operates at 9600 bps and it also transfers 6 bytes of data at a time.

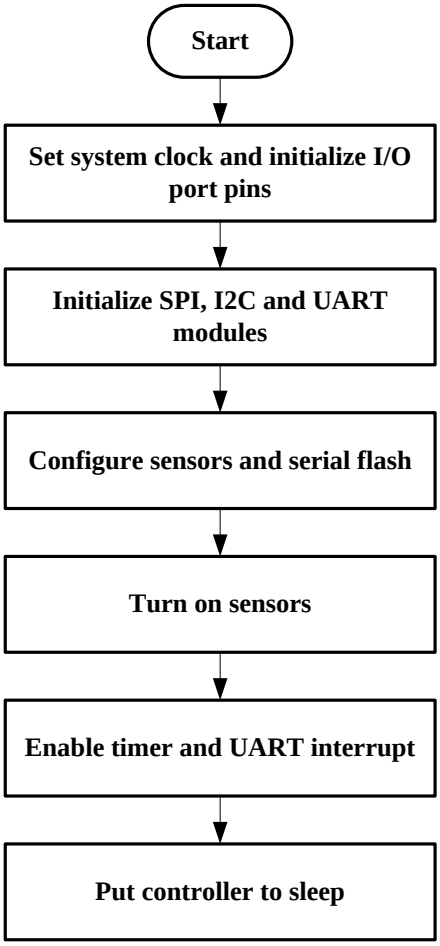


**Fig 4.1** Flowchart for the main program

The $I^2C$ module has specialized port pins, SDA (pin 23) and SCL (pin 24) and it is configured to operate at 400 kHz.

## 4.3 Configuration of sensors, serial flash, and timer

The two sensors, U4 (gyroscope) and U5 (accelerometer) are configured to operate at a full scale of ±250 °/s and ±2 g respectively and at a sampling rate of 100 Hz. Both sensors share the $I^2C$ port with the controller acting as the master and they have inbuilt FIFO which operates in a circular buffer mode with the older samples being replaced by newer ones when the buffer is full. The FIFO enables the host microcontroller to go to sleep when the sensors independently store the data. The FIFO of the accelerometer can store up to 32 samples per axis at a time while the FIFO of the gyroscope can store up to 85 samples per axis. The timer is set based on this at 0.1 ms so that 10 samples from each sensor could be comfortably read and

stored at a time. The internal filters are not enabled in either sensor so data filtering and calibration is done during signal processing.

## 4.4 Timer ISR

The timer interrupt service routine reads the FIFO count buffer of the accelerometer (FF_CNT_A) and gyroscope (FF_CNT_G), and reads the samples from each of the FIFO (represented as FIFO_A for accelerometer and FIFO_G for gyroscope). The data is transferred to serial flash after reading every sample (i.e., 6 bytes, 2 bytes per axis in the order x, y, and z ). The data is read from the accelerometer first followed by the gyroscope. After every 0.1 ms when the samples are transferred to the flash, a marker is also stored. Both the accelerometer and gyroscope data are stored in separate memory locations. The first 4 MB is reserved for gyroscope data and the next 4 MB for accelerometer data. The timer ISR is represented in Figure 4.2.

## 4.5 UART ISR

The IMU is controlled by the PC. Some of the commands that are executed by pressing specific keys are timer and sensor reset, flash memory erase, data acquisition termination and transfer. The keys and the respective commands are given in Table 4.1. Figure 4.3 shows the interrupt service routine.

**Table 4.1** UART commands

| Key | Command |
|---|---|
| ‘r’ | Timer and sensor reset |
| ‘e’ | Serial flash erase |
| ‘s’ | Data acquisition termination |
| ‘t’ | Data transfer |

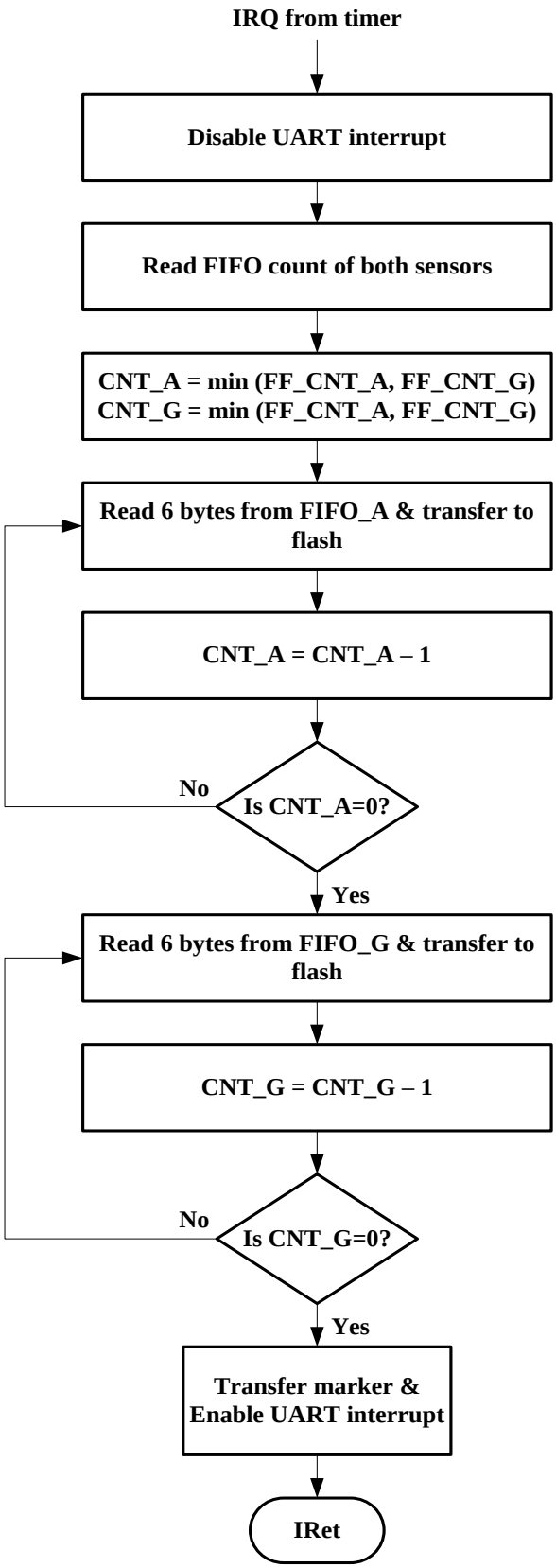


**Fig 4.2** Flowchart for timer ISR

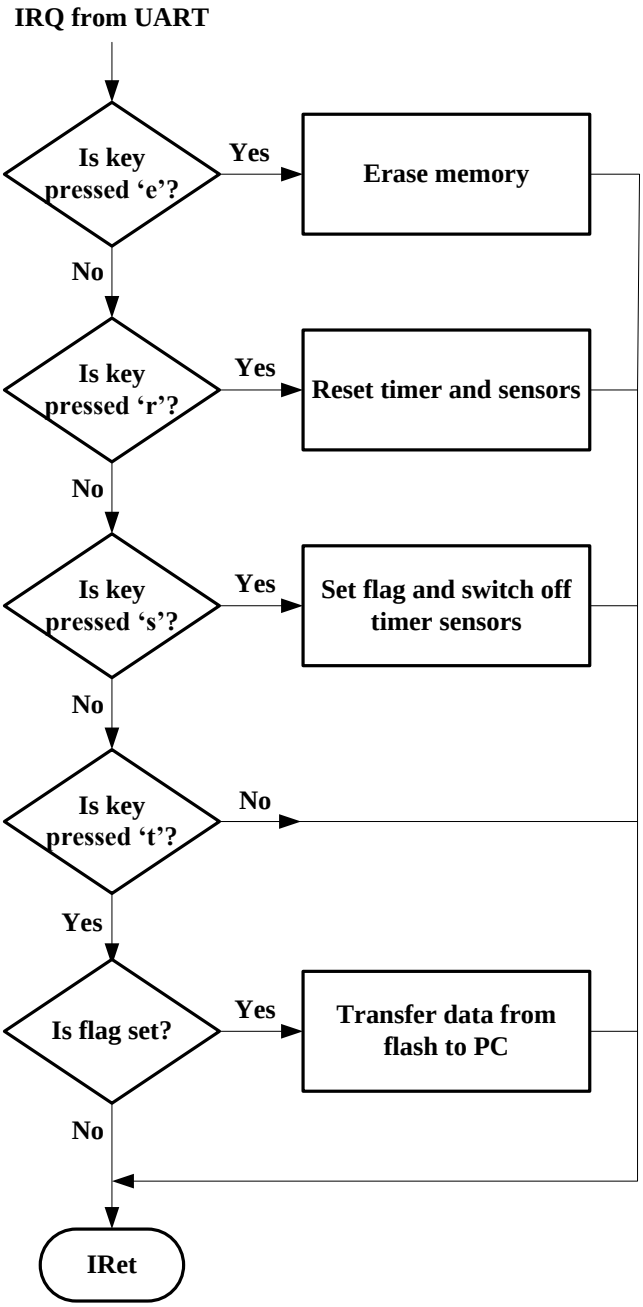


**Fig 4.3** Flowchart for UART ISR

## 4.6 Algorithm for data conversion and save

The output from the UART is in the form of a stream of ASCII characters where 6 characters represent one sample data. The gyroscope data is transferred first, then a sensor identification marker is sent next, followed by the accelerometer data. These are stored as a text file and read in MATLAB. In MATLAB data is separated by sensor and stored as two separate files and further the sensor data are separated by axis and stored in separate columns. The algorithm for converting the 6-character string to g or °/s data is given below. When MATLAB reads the text file containing the ASCII values from UART it is stored as decimal values.

Algorithm:

1. Start
2. Read data file and store in variable
3. Check for sensor identification marker
4. Split the data and store in separate variables
5. Check for 0.1 s marker
6. Remove marker and store marker location in variable
7. For each sensor data convert decimal value to binary
8. Concatenate consecutive binary values to get 16-bit 2's complement data
9. Convert 16-bit 2's complement data to binary
10. For accelerometer data multiply decimal value by 2/2^14
11. For gyroscope data multiply decimal value by 250/2^14
12. Separate data by axis
13. Using 0.1 s marker count number of samples
14. If < 10 interpolate or add required number of the last sample value at the end
15. If > 10 ignore extra samples
16. Save resultant sensor data in separate files
17. Stop

# Chapter 5
# SENSOR TEST RESULTS

## 5.1 Introduction

The output of the sensors should be ideally zero when it is not excited, however, due to internal misalignment, temperature changes or improper board mounting there may be an offset. The scale factor is a measure of the sensitivity error of the sensor and its value should be ideally 1 in this case as the input (sensor reading after conversion) and output have the same units. For the linear input-output relationship, the offset and scaling factor can be used to get the output values as [23],

$$\text{output} = \text{scale factor}\ (\text{sensor reading} - \text{offset}) \tag{5.1}$$

This chapter contains the testing procedure for the IMU sensors and the corresponding results. Testing involves comparing the output of the sensors transferred from the serial flash memory with the expected value for a known input. Testing is done to check the working of the IMU hardware and software for the given configuration.

## 5.2 Testing of the accelerometer

The accelerometer can be tested by placing it such that each of its three axes is successively aligned with 0, +g and –g acceleration. This can be achieved by placing it in six orientations, with each of the axes parallel and anti-parallel to the gravitational field. The outputs from all axes are recorded in each of the orientation. The recorded values and test results are shown in Table 5.1 and 5.2.

The testing was carried out by placing the sensor in different orientations on a table and not by referencing it along the plumbline, this was bound to cause errors in the reading. The mean and the standard deviation (SD) were taken by averaging over 2000 samples. The maximum offset observed is 0.0327 g and the scale factor is almost 1.

**Table 5.1** Accelerometer output for the six orientations

| | X | | Y | | Z | |
|---|---|---|---|---|---|---|
| Sensor orientation | Mean(g) | SD(g) | Mean(g) | SD(g) | Mean(g) | SD(g) |
| $X_{+g}$ | 1.0193 | 0.0015 | 0.0014 | 0.0013 | -0.0036 | 0.0013 |
| $X_{-g}$ | -1.0028 | 0.0043 | -0.0292 | 0.0030 | -0.0316 | 0.0041 |
| $Y_{-g}$ | 0.0070 | 0.0016 | 0.9567 | 0.0014 | -0.0220 | 0.0034 |
| $Y_{-g}$ | 0.0292 | 0.0018 | -0.9979 | 0.0016 | -0.0898 | 0.0028 |
| $Z_{+g}$ | -0.0310 | 0.0020 | -0.0632 | 0.0015 | 0.9670 | 0.0019 |
| $Z_{-g}$ | 0.0147 | 0.0016 | -0.0043 | 0.0020 | -1.0299 | 0.0022 |

**Table 5.2** Test results for accelerometer's static orientation

| Parameter | Value |
|---|---|
| $X_{off}$ | 0.0327 g |
| $Y_{off}$ | -0.0206 g |
| $Z_{off}$ | -0.0315 g |
| $X_{scale}$ | 0.9890 |
| $Y_{scale}$ | 1.0232 |
| $Z_{scale}$ | 1.0015 |

## 5.3 Testing of the gyroscope

To determine the gyroscope offset, the gyroscope is kept static and the output is averaged over a number of samples. The scale factor of an axis is determined by rotating the gyroscope by a known angle about the axis of interest and integrating the output during the period of rotation.

For gyroscope testing, a control moment gyroscope (CMG) Model 750 from Educational Control Products (ECP) available in the Control and Instrumentation Lab., Aerospace Engineering Deptartment IIT Bombay, shown in Figure 5.1 was used. The CMG houses four high resolution (16000 or 24400 counts/axis) optical encoders for gimbal rotation measurements. Using ECP's executive software for Windows platform it is possible to implement algorithms for controlling the rotation of the gimbals. Step, impulse, sinusoidal, etc. inputs of varying amplitudes can be given to the setup to rotate the gimbals by different angles and the encoder measurements can be recorded. The output from the encoder is in counts. When used with 16000 counts resolution, the output in degree is calculated by multiplying the output by a factor of 0.0225. The specifications of CMG Model 750 are given in [52].

**Fig 5.1** Control Moment Gyroscope Model 750 from Educational Control Products

The prototype board was mounted on the innermost disc of the CMG and the setup was given a sinusoidal input of 0.5 Hz frequency about each individual axis separately. The outputs were integrated over one interval (2 s) and the estimated peak value was used for the scale factor estimation. The offset was found by averaging 20 s data when the gyroscope was static. The Table 5.3 shows the test results.

The maximum offset observed is 2.9907°/s and the scale factor is almost 1.

**Table 5.3** Test results for stationary gyroscope

| Parameter | Value |
|---|---|
| $X_{off}$ | -1.4801°/s |
| $Y_{off}$ | 2.9907°/s |
| $Z_{off}$ | -0.8698°/s |
| $X_{scale}$ | 1.0279 |
| $Y_{scale}$ | 1.0129 |
| $Z_{scale}$ | 1.0135 |

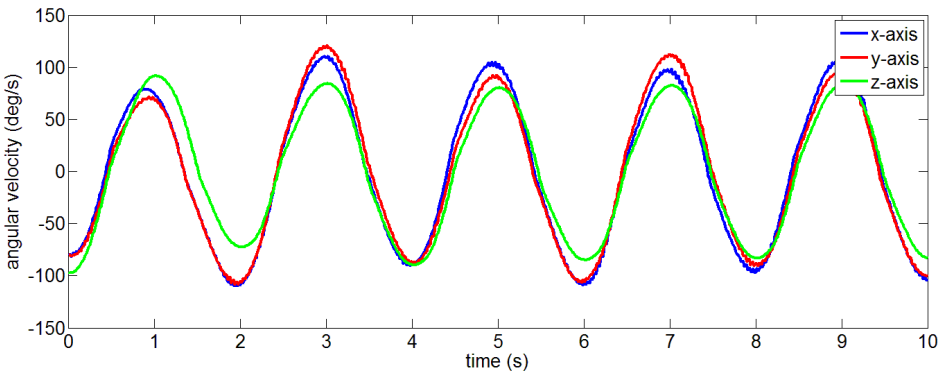


**Fig 5.2** Gyroscope for all three axes when rotated about the respective axis using CMG

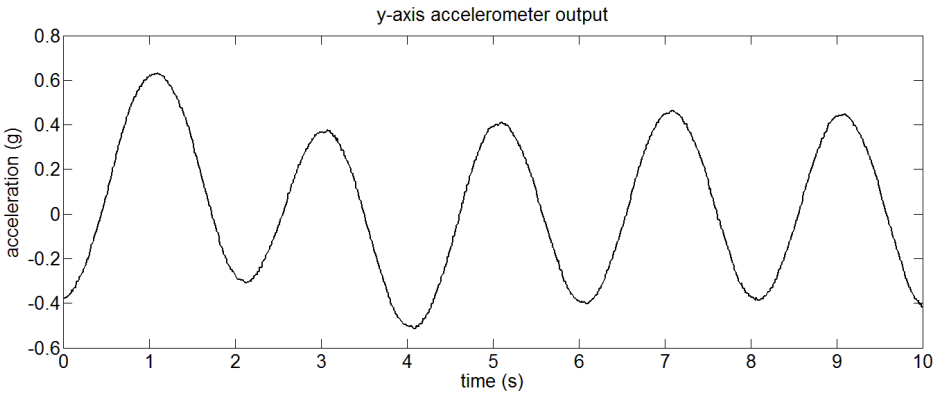


**Fig 5.3** y-axis output from accelerometer when rotated about z-axis using CMG

Figure 5.2 shows the output at the three axes when gyroscope was rotated about each of the axis. Measuring the centripetal acceleration for all axes from the angular velocity data is not feasible because the centripetal acceleration is contaminated with gravitational components during rotations. Only y-axis value during rotation about z-axis is uncontaminated and is shown in Figure 5.3. Both the figures show that the sensors respond well at 0.5 Hz which is the typical frequency of human limb movement [6].

Figure 5.4 shows a small 0.3 s section of the Figure 5.2. The crosses represent the points when the number of samples in 0.1 s at 100 Hz sampling frequency is less than 10 and to compensate the last value was added the required number of times at the end. It was observed that the gyroscope only gave 9 samples on an average for 0.1 s and the accelerometer gave 11 samples on an average and the extra samples were discarded.

Figures 5.5 to 5.7 shows the zero mean gyroscope and accelerometer out and the corresponding frequency spectrum.

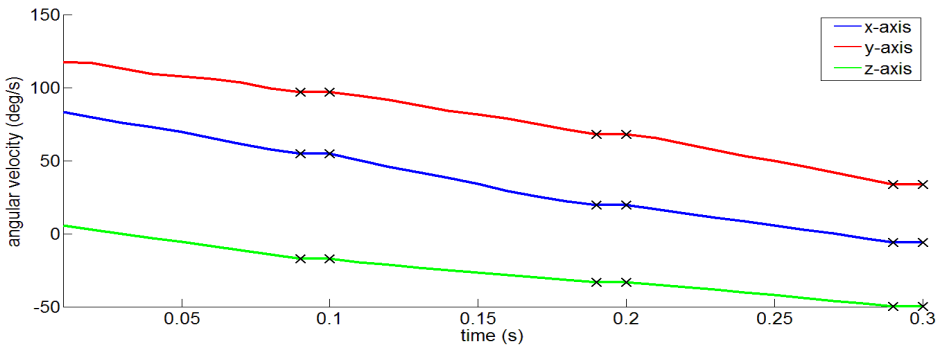

**Fig 5.4** Gyroscope output showing 0.3 s data

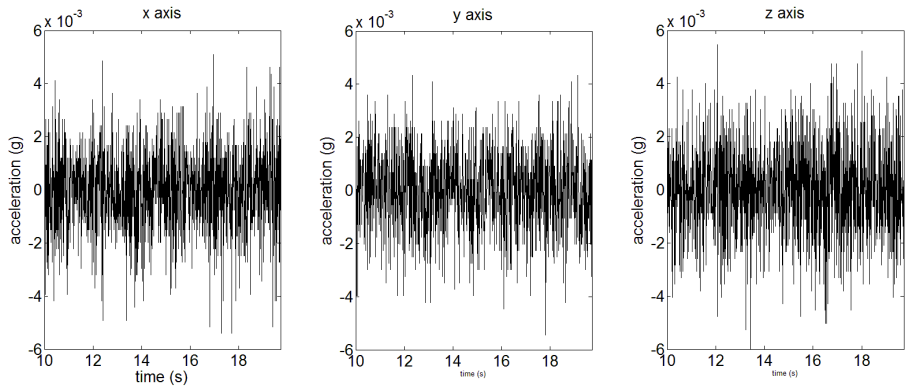


**Fig 5.5** Zero mean accelerometer outputs

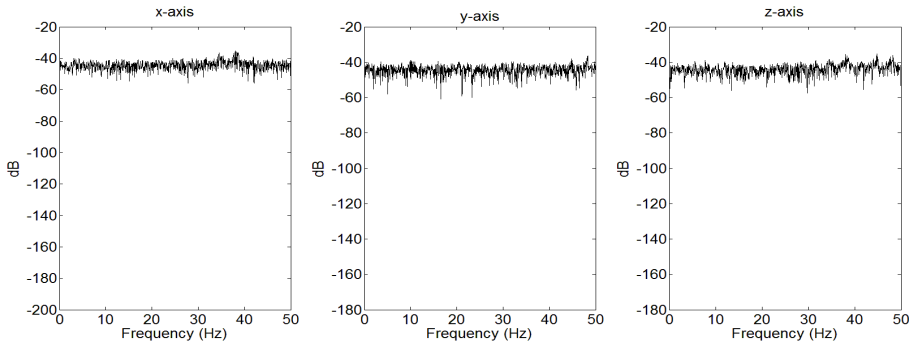


**Fig 5.6** Frequency spectrums of the zero mean accelerometer outputs

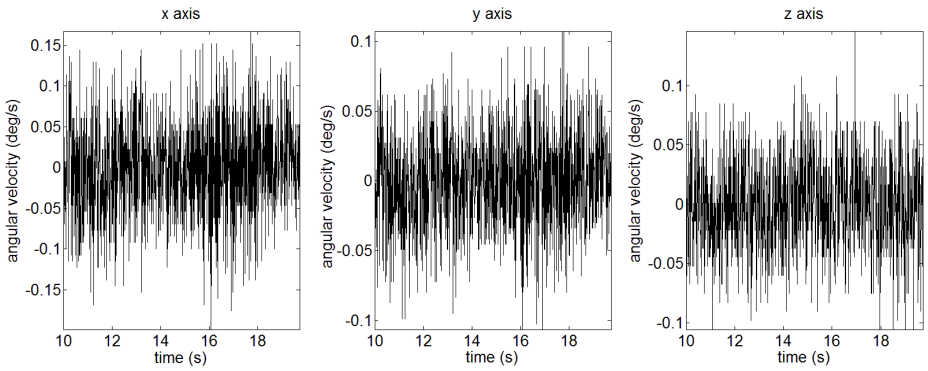


**Fig 5.7** Zero mean gyroscope outputs

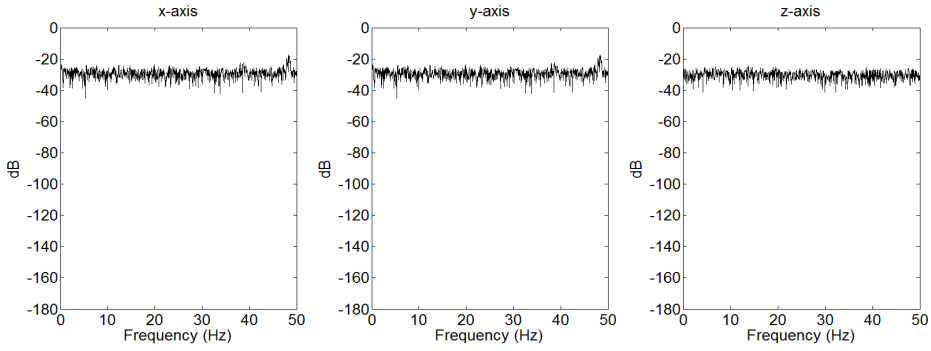


**Fig 5.8** Frequency spectrums of the zero mean gyroscope output

# Chapter 6

# FUSION OF SENSOR OUTPUTS

## 6.1 Introduction

In this chapter the algorithm for sensor fusion to determine the orientation of the IMU has been described. If the limb segment to which the IMU is attached is stationary, the accelerometer measures the local gravity vector in its body frame. This 3-D data can be used to calculate the roll and the pitch angle relative to a fixed reference frame, thus determining the orientation with respect to x and y axes. When the limb is in motion, the computed roll and pitch angles do not represent the actual orientation because of the additional movement related acceleration. This necessitates angular rate measurements for orientation estimation. While the angular rate measurements can be integrated to obtain an orientation estimate, they are prone to drift over an extended period of time. Orientation estimates from acceleration measurements do not drift over time. An extended Kalman filter is used to fuse the angular rate measurements with the orientation estimate obtained from the accelerometer data.

Orientation representation using quaternions is preferred over Euler angles because quaternion rotations do not suffer from singularities that are inherent in Euler angles. Hence, the roll and pitch angles calculated from the accelerometer is converted to a quaternion which along with the angular rate measurements is given as input to the filter as shown in Figure 6.1.

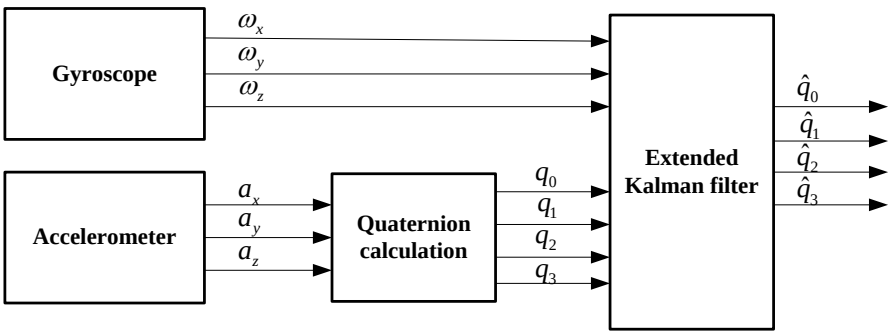


**Fig 6.1** Block diagram of sensor fusion using extended Kalman filter

## 6.2 Coordinate system

The reference coordinate system generally used for motion tracking is the earth-fixed coordinate system or the north-east-down (NED) coordinate system [6]–[20]. In this system, the earth is considered flat and non-rotating. The x and y axes, given as $x_e$ and $y_e$ lie in the earth's plane and point north and east respectively. The z-axis, $z_e$ is orthogonal to $x_e$ and $y_e$ and points downwards towards the center of the earth. In the absence of a magnetometer, we cannot measure the changes in the orientation of x and y axis when the sensor rotates about the z-axis so the reference system in this case for orientation estimation and motion tracking is only two-dimensional.

## 6.3 Representation of rotation using quaternions

The rotation in three-dimensional space for orientation tracking can be represented in different ways, Euler angles and quaternions are two of them.

The Euler angles are a set of three angles which represent the rotation of the reference frame in a fixed sequence to align it with the rotated frame [68]. The angles are known as roll ($\phi$) along X-axis, pitch ($\theta$) along Y-axis, and yaw ($\psi$) along Z-axis. Following the generally used rotation sequence 'ZYX', first the reference plane is rotated by an angle $\psi$ about the z-axis followed by a rotation of angle $\theta$ about the new y-axis and then a rotation of angle $\phi$ about the new x-axis. The integration angular velocity about each axis results in these angles. One constraint of this representation is that it has singularities at the pitch angles of $\pm 90^{\circ}$. This singularity is avoided in quaternions by the addition of a fourth element.

Euler's theorem on finite rotations states that, a rotation in a three-dimensional space could be represented as a rotation about a unit vector in that space by a specified angle [69]. Let,

$$u = \begin{bmatrix} u_1 \\ u_2 \\ u_3 \end{bmatrix} \tag{6.1}$$

be the unit vector in the three-dimensional space that represents the rotation axis and let $\alpha$ be the rotation angle. The Euler parameters are defined by

$$q_0 = \cos(\alpha / 2) \tag{6.2}$$

$$\begin{bmatrix} q_1 \\ q_2 \\ q_3 \end{bmatrix} = u\sin(\alpha/2) = \begin{bmatrix} u_1 \\ u_2 \\ u_3 \end{bmatrix} \sin(\alpha/2). \tag{6.3}$$

Because an arbitrary rotation can be described by three independent parameters, the four Euler parameters are constrained to satisfy the condition [70]

$$q_0^2 + q_1^2 + q_2^2 + q_3^2 = 1. \tag{6.4}$$

These four parameters are also called as a unit quaternion, which is commonly written as

$$q = (q_0 \; q_1 \; q_2 \; q_3) \tag{6.5}$$

where $q_0$ is the scalar part, and $[q_1 \; q_2 \; q_3]^T$ is the vector part. Another way of representing a quaternion is

$$q = q_0 + q_1\mathbf{i} + q_2\mathbf{j} + q_4\mathbf{k} \tag{6.6}$$

where **i**, **j**, and **k** denote the standard orthonormal basis for 3-D space and are defined as,

$$\mathbf{i}\cdot\mathbf{i} = \mathbf{j}\cdot\mathbf{j} = \mathbf{k}\cdot\mathbf{k} = -1 \tag{6.7}$$

$$\begin{aligned} \mathbf{i}\cdot\mathbf{j} &= \mathbf{k} = -\mathbf{j}\cdot\mathbf{i} \\ \mathbf{j}\cdot\mathbf{k} &= \mathbf{i} = -\mathbf{k}\cdot\mathbf{j} \\ \mathbf{k}\cdot\mathbf{i} &= \mathbf{j} = -\mathbf{i}\cdot\mathbf{k} \end{aligned} \tag{6.8}$$

Quaternion inverse and multiplication are the two operations needed for the application. Inverse quaternion $q^{-1}$ of $q$ is given as [70],

$$q^{-1} = \frac{q^*}{|q|^2} \tag{6.9}$$

$$q^{-1}q = qq^{-1} = 1 \tag{6.10}$$

If *s*, *q* and *r* are three quaternions, the quaternion multiplication is given as,

$$s = qr \tag{6.11}$$

where,

$$\begin{aligned} s_0 &= q_1r_1 + q_2r_2 + q_3r_3 \\ s_1 &= q_0r_1 + q_3r_2 - q_2r_3 \\ s_2 &= -q_3r_1 + q_0r_2 + q_1r_3 \\ s_3 &= q_2r_1 - q_1r_2 + q_0r_3 \end{aligned} \tag{6.12}$$

Unit quaternions can be used to perform rotation operations in three-dimensional space [70]. For any vector $v = [v_1 \; v_2 \; v_3]^T$ in the three-dimensional space, the following operation produces a vector $v'$ by rotating the vector $v$ about the axis defined by $u$ through an angle $\alpha$,

$$v' = qvq^{-1} \tag{6.13}$$

In this expression, all multiplications are quaternion multiplications, $u'$ and $v'$ are treated as pure vector quaternions whose real part is zero, and $q^{-1}$ is the inverse quaternion of $q$ [70]. Expanding the above equation, the transformation of the body coordinate $\mathbf{r}_B$ to the reference coordinate $\mathbf{r}_N$ can be given as,

$$\mathbf{r_N} = \mathbf{C_B^N r_B} \tag{6.14}$$

where $\mathbf{C_B^N}$ is the rotation matrix.

$$\mathbf{C_B^N} = \begin{bmatrix} q_0^2 + q_1^2 - q_2^2 - q_3^2 & 2q_1q_2 - 2q_0q_3 & 2q_1q_3 + 2q_0q_2 \\ 2q_1q_2 + 2q_0q_3 & q_0^2 - q_1^2 + q_2^2 - q_3^2 & 2q_2q_3 - 2q_0q_1 \\ 2q_1q_3 - 2q_0q_2 & 2q_2q_3 + 2q_0q_1 & q_0^2 - q_1^2 - q_2^2 + q_3^2 \end{bmatrix} \tag{6.15}$$

## 6.4 Quaternion based extended Kalman filter

The extended Kalman filter algorithm given by Bachmann *et al*. [6] has been used. They have used, QUEST (quaternion estimate) algorithm has been used to compute the quaternion from accelerometer and magnetometer outputs. In the absence of magnetometer, in our application the quaternions have been estimated directly from the accelerometer data.

### *6.4.1 Filter basics*

The Kalman filter was originally designed to solve the minimum mean-square estimation problem using state space methods, where the measurements are included as functions of the state [68]. The Kalman filter is a recursive filter that has a prediction stage and a correction stage. In the prediction stage the current state vector of the system is predicted from the previous state vector along with its uncertainties. When the next measurement arrives, the estimated state vector is updated using weighted average, with more weight being given to estimates with higher certainties.

For a linear, discrete-time dynamical system the system state equation and measurement equation are given as [68],

$$\mathbf{x}_{k+1} = F_k\mathbf{x}_k + \boldsymbol{w}_k \tag{6.16}$$

$$\mathbf{z}_k = C_k\mathbf{x}_k + \boldsymbol{v}_k \tag{6.17}$$

where, $\mathbf{x}_k$ $(n\times1)$ is the process state vector at time $t_k$, $\boldsymbol{F}$ $(n\times n)$ is the state transition matrix relating $\mathbf{x}_k$ to $\mathbf{x}_{k+1}$, $\mathbf{z}_k$ $(n\times1)$ is the measurement vector at time $t_k$ or the $k^{th}$ sample, and $\boldsymbol{C}$ $(n\times n)$ is the measurement matrix. It is assumed that $\boldsymbol{w}_k$, the process noise and $\boldsymbol{v}_k$, the measurement noise are statistically independent discrete white noise with zero mean and known covariance matrices $\boldsymbol{Q}_k$ and $\boldsymbol{R}_k$, respectively.

The extended Kalman filter is a modified Kalman filter algorithm for systems with non-linear dynamical system state equation and measurement equation, given as [68],

$$\mathbf{x}_{k+1} = f(\mathbf{x}_k, t_k) + \boldsymbol{w}_k \tag{6.18}$$

$$\mathbf{z}_k = c(\mathbf{x}_k, t_k) + \boldsymbol{v}_k \tag{6.19}$$

The equations are linearized by taking their first order Taylor's series approximates and used in the Kalman filter recussion.

The Kalman filter recursion solves five equations to estimate the state vector using the previous estimate and a weighted version of the difference between the

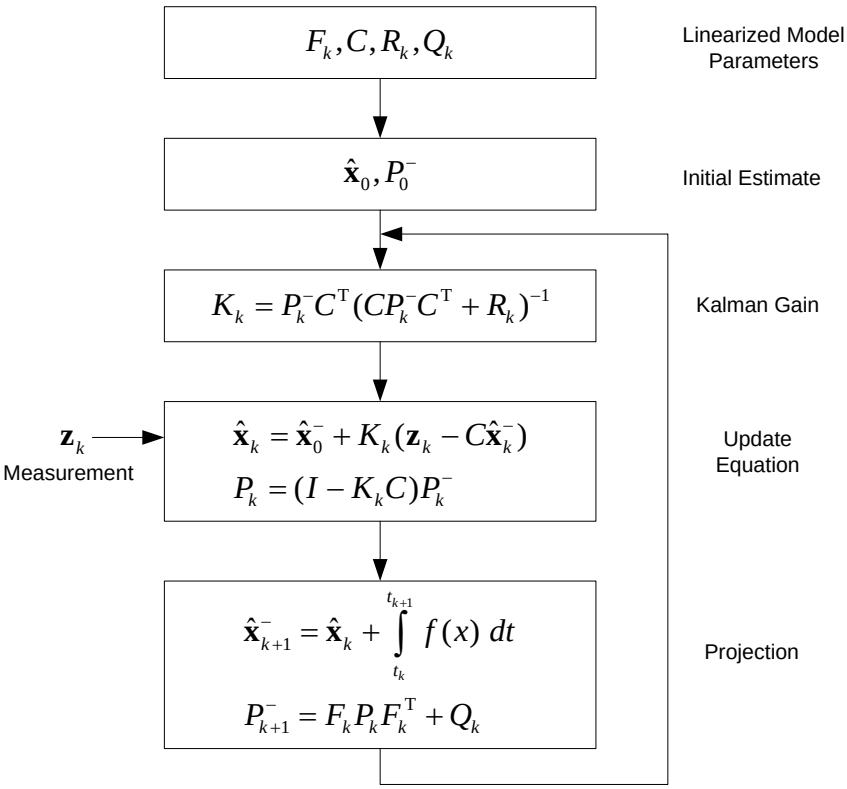


**Fig 6.2** The extended Kalman filter recursion

measurement and the estimate. $K_{k\ (n\times n)}$ is the gain matrix which is updated at every step, it is a function of the relative certainty of the measurements and current state estimate. For a high gain, more weight is placed on the measurements, and thus the filter follows them more closely. For a low gain, the filter follows the estimates more closely, smoothing out noise but decreasing the responsiveness. and $\boldsymbol{P}_{k\ (n\times n)}$ is the error covariance matrix which is a measure of the estimated accuracy of the state estimate, the superscript $^-$ represents a*priori* state. Figure 6.2 shows the recursion of the extended Kalman filter.

*6.4.2 Quaternion calculation from accelerometer output*

The roll angle ($\phi$) and the pitch angle ($\theta$) can be calculated from the accelerometer output as [71],

$$\phi(k)=\begin{cases}\tan^{-1}\left(\dfrac{a_y(k)}{a_z(k)}\right) & \text{for } a_z(k)<0\\ -\pi+\tan^{-1}\left(\dfrac{a_y(k)}{a_z(k)}\right) & \text{for } a_z(k)>0 \text{ and } a_y(k)>0\\ \pi+\tan^{-1}\left(\dfrac{a_y(k)}{a_z(k)}\right) & \text{for } a_z(k)>0 \text{ and } a_y(k)<0\end{cases} \tag{6.20}$$

$$\theta(k)=\tan^{-1}\left(\frac{a_z(k)}{\sqrt{a_y^2(k)+a_z^2(k)}}\right) \tag{6.21}$$

from the roll and the pitch angles, the quaternion can be obtained using,

$$\begin{aligned} q_0 &= \cos(\theta/2)\cos(\phi/2)\\ q_1 &= \cos(\theta/2)\sin(\phi/2)\\ q_2 &= \sin(\theta/2)\cos(\phi/2)\\ q_3 &= -\sin(\theta/2)\sin(\phi/2)\end{aligned} \tag{6.22}$$

At every time step *k*, the quaternion is obtained from the equations 6.16 − 6.18 and given as input to the extended Kalman filter.

*6.4.3 Filter process model*

A process model representing the dynamics of the human limb motion is give by Bachmann *et al*. [6] (Figure 6.1). The angular velocity $\omega$ is thus modeled as a colored

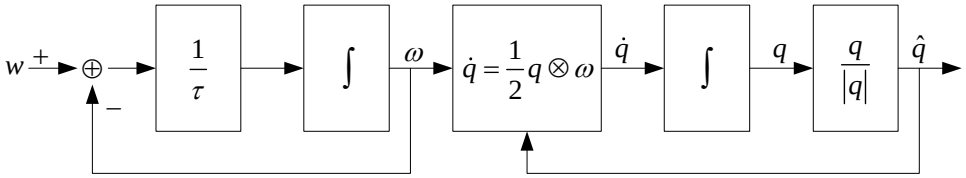


**Fig 6.1** Filter process model [6]

noise generated by a linear system with white noise $w$ input. The time constant $\tau$ determines how fast a limb segment can move in a typical human motion condition. The angular velocity and the quaternion derivative $\dot{q}$ are related by the identity [70],

$$\dot{q} = \frac{1}{2} q \otimes \omega \tag{6.23}$$

where $\otimes$ represents the quaternion multiplication.

*6.4.4 Filter design*

The state equation for the filter is derived from the process model and is thus the state vector is a 7-D vector. It has two parts, the first part being the 3-D angular rate vector $\omega = \begin{bmatrix} \omega_x & \omega_y & \omega_z \end{bmatrix}^{\mathrm{T}}$ or represented as $\omega = \begin{bmatrix} \omega_1 & \omega_2 & \omega_3 \end{bmatrix}^{\mathrm{T}}$ and the next is the 4-D quaternion $q = \begin{bmatrix} q_0 & q_1 & q_2 & q_3 \end{bmatrix}^{\mathrm{T}}$. The process model equations are given as,

$$\dot{\omega}_i = \frac{1}{\tau_i}(-\omega_i + w) \text{ for } i = 1,2,3 \tag{6.24}$$

$$\dot{q} = \frac{1}{2}(q \otimes \omega) \tag{6.25}$$

where $w$ is the white Gaussian noise. Thus for the 7-D state vector

$$\begin{bmatrix} x_1 \\ x_2 \\ x_3 \end{bmatrix} = \begin{bmatrix} \omega_1 \\ \omega_2 \\ \omega_3 \end{bmatrix} = \omega, \quad \begin{bmatrix} x_4 \\ x_5 \\ x_6 \\ x_7 \end{bmatrix} = \begin{bmatrix} q_0 \\ q_1 \\ q_2 \\ q_3 \end{bmatrix} = q$$

The state equation is given as,

$$\begin{bmatrix} \dot{x}_1 \\ \dot{x}_2 \\ \dot{x}_3 \\ \dot{x}_4 \\ \dot{x}_5 \\ \dot{x}_6 \\ \dot{x}_7 \end{bmatrix} = \begin{bmatrix} \frac{1}{\tau_1}(-x_1 + w_1) \\ \frac{1}{\tau_2}(-x_2 + w_3) \\ \frac{1}{\tau_3}(-x_3 + w_3) \\ \frac{1}{2}(-x_1x_5 - x_2x_6 - x_3x_7) \\ \frac{1}{2}(x_1x_4 - x_2x_7 + x_3x_6) \\ \frac{1}{2}(x_1x_7 + x_2x_4 - x_3x_5) \\ \frac{1}{2}(-x_1x_6 + x_2x_5 + x_3x_4) \end{bmatrix} \tag{6.26}$$

Equation 6.22 for the time step *k* can be written as,

$$\dot{\mathbf{x}}_k = f(x_k, t_k) + w(t_k) \tag{6.27}$$

The state transition matrix is then derived by linearizing the function $f(x_k, t_k)$ along the currently estimated trajectory $\hat{\mathbf{x}}_k$ as,

$$F_k = \left.\frac{\partial f(x_k, t_k)}{\partial x}\right|_{x=\hat{x}_k} \tag{6.28}$$

after linearization, the continuous-time model is discretized and given as,

$$F_k = \begin{bmatrix} e^{-\frac{\delta}{\tau_1}} & 0 & 0 & 0 & 0 & 0 & 0 \\ 0 & e^{-\frac{\delta}{\tau_2}} & 0 & 0 & 0 & 0 & 0 \\ 0 & 0 & e^{-\frac{\delta}{\tau_3}} & 0 & 0 & 0 & 0 \\ -\frac{\hat{x}_5\delta}{2} & -\frac{\hat{x}_2\delta}{2} & -\frac{\hat{x}_7\delta}{2} & 1 & -\frac{\hat{x}_1\delta}{2} & -\frac{\hat{x}_2\delta}{2} & -\frac{\hat{x}_3\delta}{2} \\ \frac{\hat{x}_4\delta}{2} & -\frac{\hat{x}_7\delta}{2} & \frac{\hat{x}_6\delta}{2} & \frac{\hat{x}_1\delta}{2} & 1 & \frac{\hat{x}_3\delta}{2} & -\frac{\hat{x}_2\delta}{2} \\ \frac{\hat{x}_7\delta}{2} & \frac{\hat{x}_4\delta}{2} & -\frac{\hat{x}_5\delta}{2} & \frac{\hat{x}_2\delta}{2} & -\frac{\hat{x}_3\delta}{2} & 1 & \frac{\hat{x}_1\delta}{2} \\ -\frac{\hat{x}_6\delta}{2} & \frac{\hat{x}_5\delta}{2} & \frac{\hat{x}_4\delta}{2} & \frac{\hat{x}_3\delta}{2} & \frac{\hat{x}_2\delta}{2} & -\frac{\hat{x}_1\delta}{2} & 1 \end{bmatrix} \tag{6.29}$$

where $\delta$ is the sampling interval and is equal to 0.01 s also, $\tau_i = 0.5$ s from the process model. The process noise covariance matrix $Q_k = E\left[ w_k w_k^{\mathrm{T}} \right]$ is calculated as

$$Q_k = \begin{bmatrix} 0.016 & 0 & 0 & 0 & 0 & 0 & 0 \\ 0 & 0.016 & 0 & 0 & 0 & 0 & 0 \\ 0 & 0 & 0.016 & 0 & 0 & 0 & 0 \\ 0 & 0 & 0 & 0 & 0 & 0 & 0 \\ 0 & 0 & 0 & 0 & 0 & 0 & 0 \\ 0 & 0 & 0 & 0 & 0 & 0 & 0 \\ 0 & 0 & 0 & 0 & 0 & 0 & 0 \end{bmatrix}$$

where the variance of the white Gaussian noise $w_k$ is obtained from the process model. The measurement equation is linear as the estimated output can be compared with the output from the angular rate measurements and the quaternions calculated from the accelerometer data. Thus, using equation 6.17

$$\mathbf{z}_k = C\mathbf{x}_k + v_k$$

where $C$ is a $7 \times 7$ identity matrix and the measurement noise covariance matrix $R_k = E\left[ v_k v_k^{\mathrm{T}} \right]$ is experimentally determined as

$$R_k = \begin{bmatrix} 0.2 & 0 & 0 & 0 & 0 & 0 & 0 \\ 0 & 0.2 & 0 & 0 & 0 & 0 & 0 \\ 0 & 0 & 0.2 & 0 & 0 & 0 & 0 \\ 0 & 0 & 0 & 0.00001 & 0 & 0 & 0 \\ 0 & 0 & 0 & 0 & 0.00001 & 0 & 0 \\ 0 & 0 & 0 & 0 & 0 & 0.00001 & 0 \\ 0 & 0 & 0 & 0 & 0 & 0 & 0.00001 \end{bmatrix}$$

The matrices $F_k$ , $C$, $R_k$, and $Q_k$ are given as input to the extended Kalman filter recursion along with the initial state vector $\hat{\mathbf{x}}_0$ and initial error covariance matrix $P_0^-$.

## 6.5 Results

The output of the gyroscope when placed on the control moment gyroscope was used for the testing the accuracy of the algorithm. The pre-calculated quaternion values were obtained from the corresponding accelerometer output. The Kalman gain is determined such that the sum of squared errors is minimized which is observed as the convergence of the trace of the error covariance matrix. Figure 6.3 shows the trace and it can be seen that the sum of squared errors reaches a steady state after

approximately 0.03 s. Figures 6.4 and 6.5 show the comparison between the estimated roll and pitch output from the extended Kalman filter, calculated output by integration of the corresponding angular velocity, and the actual output from the optical encoder output of the CMG. Finally Table 6.1 shows the correlation coefficient and the

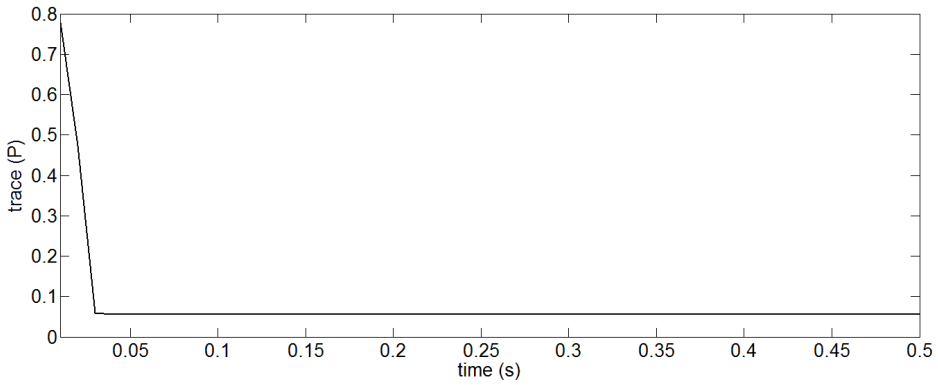


**Fig 6.3** Trace of error covariance matrix

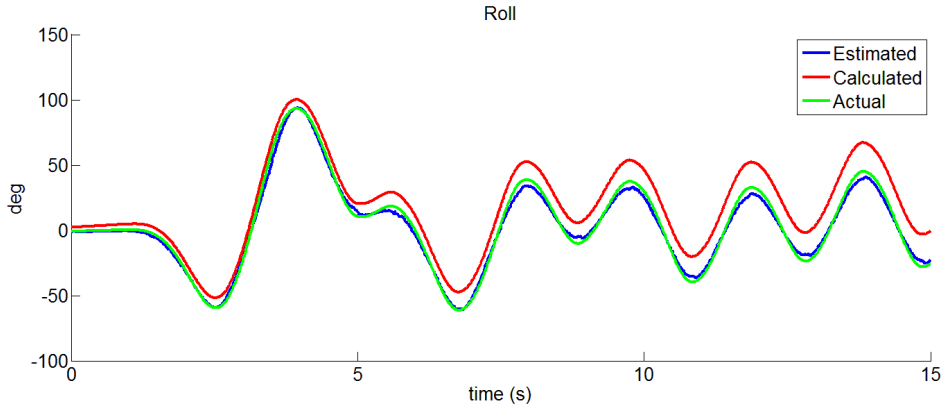


**Fig 6.4** Roll output

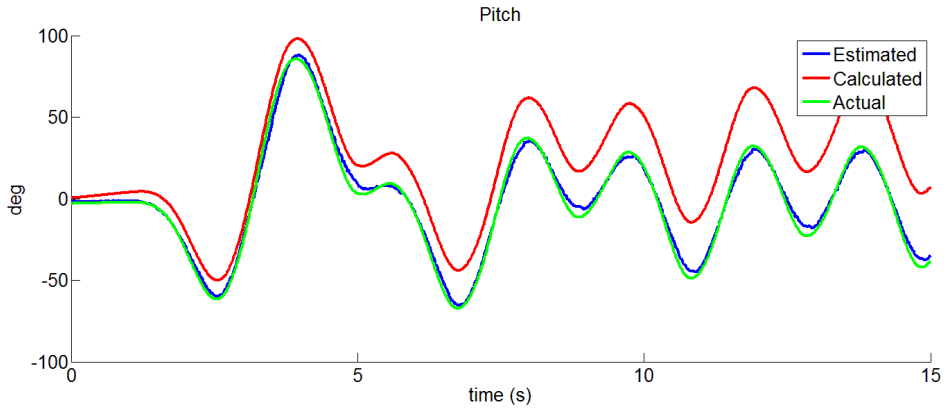


**Fig 6.5** Pitch output

**Table 6.1** Correlation coefficient and RMS error between estimated and actual output

| Angle | Corr. Coeff. | Rel. RMS error (%) |
|---|---|---|
| Roll | 0.998 | 5.5 |
| Pitch | 0.996 | 6.5 |

relative RMS error between the estimated value and actual output. It can be thus seen that the output from the filter has a high correlation with the actual output and the relative RMS error is about 6%.

# Chapter 7
# SUMMARY AND SUGGESTIONS

## 7.1 Summary

The objective of this project was to develop an inertial measurement unit for motion and posture tracking application for assisted living. These small size units are stand alone devices that do not require external reference for its operation. IMU has a triaxial accelerometer and a triaxial gyroscope for three-degree linear motion capture and two-degree orientation capture. These sensors suffer from extrinsic and intrinsic noises that cause offset and drift during integration. Calibration and fusion algorithms are used to reduce these errors.

The triaxial accelerometer (MMA8451Q) and gyroscope (IMU3000A) are interfaced with a microcontroller (PIC24FJ64GB004) which acts as the master device and controls the data acquisition, storage, and transfer. A 64 Mb serial flash is used as the onboard memory. When the sampling rate is 100 Hz, data could be stored for 2 hours. The accelerometer and gyroscope operate at ±2 g and ±250°/s. The data of both the sensors are stored in the respective FIFO and it is read by the controller at every 0.1 s. This is controlled by a timer and the controller is put to sleep in between to save power. Data is transferred using RS232 to PC where the signal processing is carried out in MATLAB.

For sensor calibration, the null point and scale factor for both the sensors are determined and their response was tested for 0.5 Hz sinusoidal input which is the typical frequency of human limb motion.

The quaternion based extended Kalman filter algorithm was implemented for orientation estimation by fusing the gyroscope output with a pre-calculated quaternion obtained from the accelerometer data. The data recorded using the control moment gyroscope was used for testing and the results showed 99% correlation with the actual signal

## 7.2 Suggestions for future work

Modifications could be made in the IMU design for wireless or USB data transmission. Power consumption of the circuit could be reduced by using an optimal regulator. As the processing is done in PC the controller could be optimized. A smaller and more power efficient controller could be used. The variable sampling rate problem could be solved by using a single chip multi-sensor module. And further, a triaxial magnetometer could be used to further increase the scope of the device.

# Appendix A

# COMPONENT LIST

| Component designator | Component description | Part number / value | Quantity |
|---|---|---|---|
| C1, C2, C3, C4, C5, C6, C7, C8, C9, C10, C12, C16, C15, C17, C18, C20, C22 | Capacitor, ceramic, surface mounted | 0.1 μF | 17 |
| C3 | Capacitor, ceramic, surface mounted | 10 μF | 1 |
| C11 | Capacitor, ceramic, surface mounted | 10 nF | 1 |
| C13 | Capacitor, ceramic, surface mounted | 2.2 nF | 1 |
| C14 | Capacitor, ceramic, surface mounted | 4.7 μF | 1 |
| C19 | Capacitor, ceramic, surface mounted | 1 μF | 1 |
| C21, C23 | Capacitor, electrolytic, surface mounted | 100 μF | 2 |
| R1, R4 | Resistor, surface mounted | 10 kΩ | 2 |
| R2 | Resistor, surface mounted | 100 Ω | 1 |
| R5, R6, R7, R8 | Resistor, surface mounted | 4.7 kΩ | 4 |
| R9 | Resistor, surface mounted | 2.2 kΩ | 1 |
| R10 | Resistor, surface mounted | 5.1 kΩ | 1 |
| J1 | Connector, 1-pin | CON1 | 1 |
| J2, J3 | Connector, 3-pin | CON3 | 2 |
| J4 | Connector, 2-pin | CON2 | 1 |
| J5 | Connector, 6-pin | CON6 | 1 |
| SW1 | SPDT | SW1 | 1 |
| DEBUG | Connector, 5-pin | CON5 | 1 |
| USB | Connector, 5-pin | CON5 | 1 |
| U1 | IC, microcontroller, 44-pin, TQFP | 24FJ64GB004 | 1 |
| U2 | IC, RS232 driver, 16-pin, SSOP | SP3232E | 1 |
| U3 | IC, serial flash, 8-pin, SOIC | SST25VF064C | 1 |
| U4 | IC, triaxial gyroscope, 24-pin, QFN | IMU3000A | 1 |
| U5 | IC, triaxial accelerometer, 16-pin, QFN | MMA8451Q | 1 |
| U6 | IC, regulator, 3-pin, SOT | LM1117 | 1 |

# Appendix B

# SCHEMATIC DIAGRAM OF THE IMU

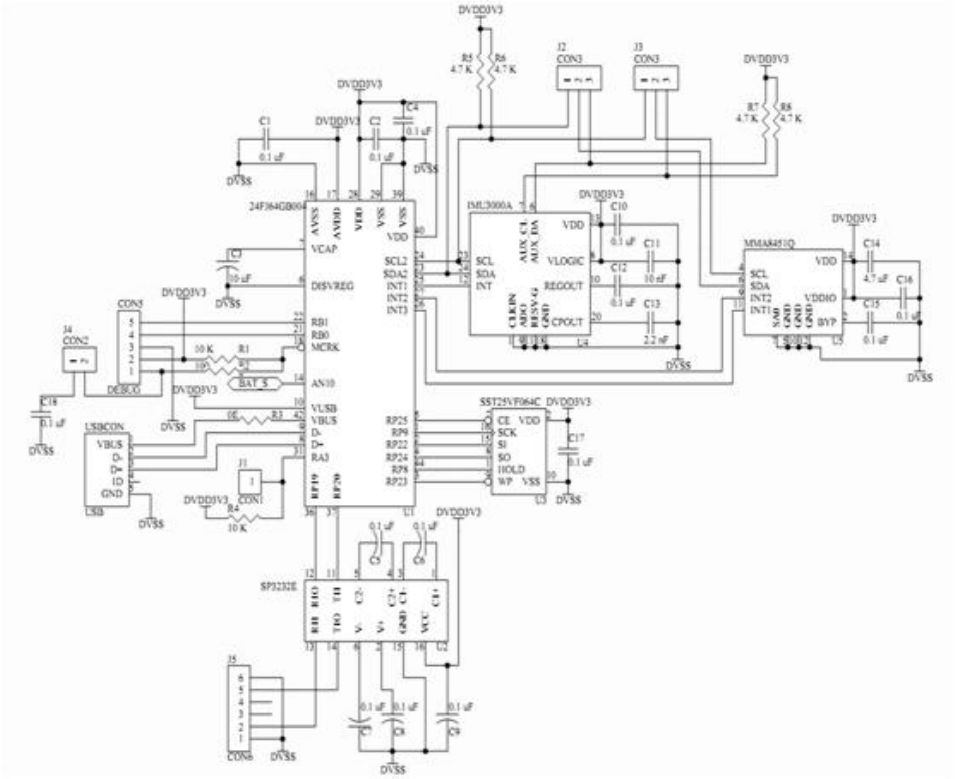


**Fig B.1** Schematic diagram of the IMU

# Appendix C

# PCB LAYOUT OF THE IMU

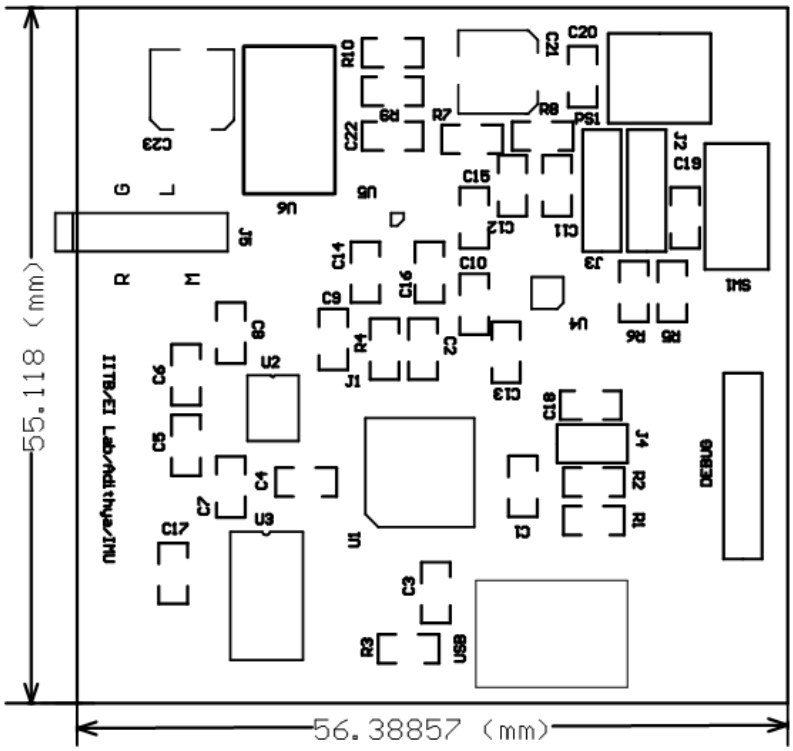


**Fig C.1** Top overlay layer of the IMU (56 mm x 55 mm)

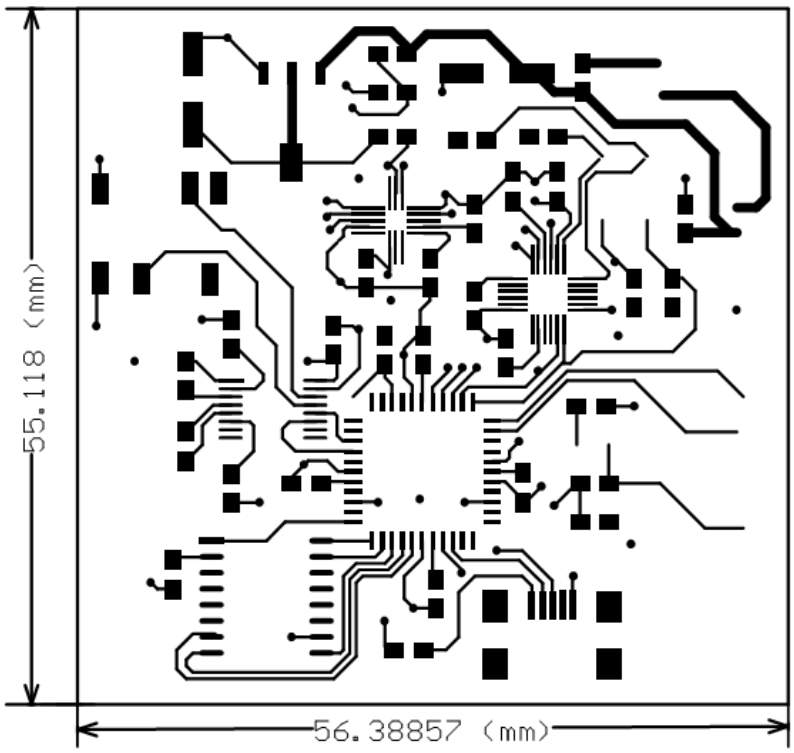


**Fig C.2** Top layer of the IMU (56 mm x 55 mm)

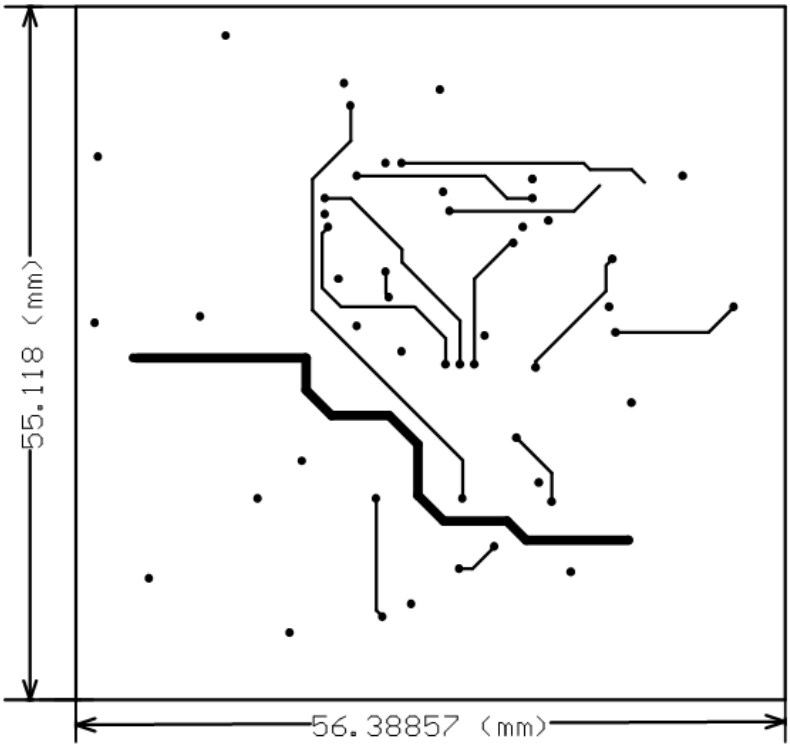


**Fig C.3** Bottom layer of the IMU (56 mm x 55 mm)

# REFERENCE


[1] G. Welch, G. Bishop, L. Vicci, S. Brumback, K. Keller, and D. Colucci, "The HiBall tracker: high-performance wide-area tracking for virtual and augmented environments," in *Proc. ACM Symp. Virtual Reality Softw. Technol.*, London, U.K., Dec. 1999, pp. 1–11.

[2] W. Korb, D. Engel, R. Boesecke, G. Eggers, B. Kotrikova, R. Marmulla, J. Raczkowsky, H. Worn, J. Muhling, and S. Hassfeld (2003, Apr.). Development and first patient trial of a surgical robot for complex trajectory milling. *Comput. Aided Surg*. [Online]. *8(5)*. 247–256. Available: http://www.ncbi.nlm.nih.gov/pubmed/15529954?dopt=Citation

[3] T. Lee and A. Mihailidis, "An intelligent emergency response system: preliminary development and testing of automated fall detection," *Telemed and Telecare*, vol. 11, pp. 194–198, 2005.

[4] Vicon, "Case study: The dance of love", Available: http://www.vicon.com/company/documents/Northumbria_owres.pdf, downloaded on 1st June 2012.

[5] Acoustic motion capture, by O. Gabai and H. Primo. (2011, Jan. 13). *Patent Application 20110009194* [Online]. Available: http://appft1.uspto.gov/netacgi/nph-Parser?Sect1=PTO1&Sect2=HITOFF&d=PG01&p=1&u=/netahtml/PTO/srchnum.html&r=1&f=G&l=50&s1=20110009194.PGNR.

[6] X. Yun and R. Bachmann, "Design, implementation, and experimental results of a quaternion-based Kalman filter for human body motion tracking," *IEEE Trans. Robotics.*, vol. 22, no. 6, pp. 1216–1227, Dec. 2006.

[7] A. Gallagher, Y. Matsuoka, and W. T. Ang, "An efficient real-time human posture tracking algorithm using low-cost inertial and magnetic sensors," in *Proc. IEEE Int. Conf. Robot. Autom.*, Sendai, Japan, Sep. 28–Oct. 2, 2004, pp. 2967–2972.

[8] J. S. Wang, Y. L. Hsu, and J. N. Liu, "An inertial measurement unit based pen with a trajectory reconstruction algorithm and its applications," *IEEE Trans. Ind. Electron.*, vol. 57, no. 10, pp. 3508–3521, Oct. 2010.

[9] R. Zhu and Z. Zhou, “A real-time articulated human motion tracking using tri-axis inertial/magnetic sensors package,” *IEEE Trans. Neural Syst. Rehab. Eng.*, vol. 12, no. 2, pp. 295–302, Jun. 2004.

[10] J. Lee and I. Ha, “Sensor fusion and calibration for motion captures using accelerometers,” in *Proc. IEEE Int. Conf. Robot. Autom.*, Detroit, MI, May 1999, pp. 1954–1959.

[11] D. Gebre-Egziabher, G. H. Klkaim, J. Powell, and B. W. Parkinson, “A gyro-free quaternion-based attitude determination system suitable for implementation using low cost sensors,” in *Proc. IEEE Position Location, Navig. Symp.*, San Diego, CA, Mar. 2000, pp. 185 –192.

[12] T. Chin-Woo, S. Park, K. Mostov, and P. Varaiya, “Design of gyro-scope-free navigation systems,” in *Proc. IEEE Intell. Transport. Syst.*, Oakland, CA, Aug. 2001, pp. 286–291.

[13] A. M. Sabatini, C. Martelloni, S. Scapellato, and F. Cavallo, “Assessment of walking features from foot inertial sensing,” IEEE *Trans. Aerosp. Electron. Syst.*, vol. 52, no. 3, pp. 486–494, Mar. 2005.

[14] J. L. Marins, X. Yun, E. R. Bachmann, R. B. McGhee, and M. J. Zyda, “An extended Kalman filter for quaternion-based orientation estimation using MARG sensors,” in *Proc. IEEE/RSJ Int. Conf. Intell. Robots Syst.*, Maui, HI, Oct. 2001, pp. 2003 –2011.

[15] X. Yun, M. Lizarraga, E. Bachmann, and R. McGhee, “An improved quaternion-based Kalman filter for real-time tracking of rigid body orientation,” in *Proc. IEEE/RSJ Int. Conf. Intell. Robots Syst.*, Las Vegas, NV, Oct. 2003, vol. 2, pp. 27–31.

[16] X. Yun, C. Aparicio, E. R. Bachmann, and R. B. McGhee, “Implementation and experimental results of a quaternion-based Kalman filter for human body motion tracking,” in *Proc. IEEE Int. Conf. Robot. Autom.*, Barcelona, Spain, Apr. 2005, pp. 317–322.

[17] D. Roetenberg, H. J. Luinge, T. M. Baten, and P. H. Veltink, “Compensation of magnetic disturbances improves inertial and magnetic sensing of human body segment orientation,” *IEEE Trans. Neural Syst. Rehab. Eng.*, vol. 13, no. 3, pp. 395–405, Sep. 2005.

[18] H. Zhou, H. Hu, and N. Harris, "Application of wearable inertial sensors in stroke rehabilitation," in *Proc. IEEE Int. Conf. Eng. Med. Bio.*, Shangai, China, Sep. 1–4, 2005, pp. 2967–2972.

[19] E. Haeuber, M. Shaughnessy, L. W. Forrester, K. L. Coleman, and R. F. Macko, "Accelerometer monitoring of home- and community-based ambulatory activity after stroke," *J. Arch. Phys. Med. Rehabil.*, vol. 85, no. 12, pp. 1997–2001, Dec., 2004.

[20] H. Zheng, "Web-based monitoring system for home-based rehabilitation with stroke patients," in *Proc. IEEE Symp. Comp. Med. Syst.*, Washington DC, USA, June 2005, pp. 419–424.

[21] A. Weiss, S. Sharifi, M. Plotnik, J. P. P. van Vugt, N. Giladi, and J. M. Hausdorff, "Toward automated, at-home assessment of mobility among patients with Parkinson disease, using a body-worn accelerometer," *J. Neurorehabilitation Neural Repair*, vol. 25, pp. 810–818, Nov/Dec., 2011.

[22] L. Cunningham, S. Mason, C. Nugent, G. Moore, D. Finlay, and D. Craig, "Home-based monitoring and assessment of parkinson's disease," *IEEE Trans. Inform. Technol. Biomedicine*, vol. 15, no. 1, pp. 47–53, Jan., 2011.

[23] R. Begg, E. Charry, M. Paliniswami, and K. Hill, "Measuring toe clearance using a wireless inetial sensong device," in *IEEE ISSNIP Conf.*, Sydney, 2008, pp. 375–380.

[24] C. N. Huang, C. Y. Chiang, G. C. Chen, S. J. Hsu, W. C. Chu, and C. T. Chan , "Fall detection system for healthcare quality improvement in residential care facilities," *J. Med. Biol. Eng.*, vol. 30, no. 4, pp. 247–252, Jul., 2010.

[25] J. M. Churko, A. Mehr, A. G. Linassi, and A. Dinh, "Sensor evaluation for tracking upper extremity prosthesis movements in a virtual environment," in *Proc. IEEE EMBS Conf.*, Minneapolis, Minnesota, 2009, pp. 2392–2395.

[26] F. Lorussi, A. Tognetti, N. Carbonaro, G. Anania, and D. D. Rossi, "Enhancing the performance of upper limb gesture reconstruction through sensory function," in *Proc. IEEE EMBS Conf.*, Boston, Massachusetts, 2011, pp. 3496–3499.

[27] M. El-Gohary, L. Holmstrom, J. Huisinga, E. King, J. McNames, and F. Horak, "Upper limb joint angle tracking with inertial sensors," in *Proc. IEEE EMBS Conf.*, Boston, Massachusetts, 2011, pp. 5629–5632.

[28] P. J. Hauri and J. Wisbey, "Wrist actigraphy in insomnia," *Sleep*, vol. 15, no. 4, pp. 293–301, 1992.

[29] D. Minors and T. Akerstedt. (1996, May). The difference between activity when in bed and out of bed. *Chronobiol. Int*. [online]. *13(1)*, pp. 13–27, Available: http://www.ncbi.nlm.nih.gov/sites/entrez?cmd=Retrieve&db=pubmed&dopt=Abstract&list_uids=8761934

[30] V. Collado-Seidel and J. Kazenwadel. (1999, Jan.). A controlled study of additional sr-L-dopa in L-dopa-responsive restless legs syndrome with late-night symptoms. *Neurology*. [Online]. *52(2)*. pp. 285–290, Available: http://www.neurology.org/content/52/2/285.abstract?sid=c03de637-2863-4da9960f-7a26f2c55a14

[31] F. Bagala, C. Becker, A. Cappello, L. Chiari, and K. Aminian (2012, Apr.) Evaluation of accelerometer-based fall detection algorithms on real-world falls. *PLoS One*. [Online]. *7(5)*. 91–99. Available: http://www.plosone.org/article/info%3Adoi%2F10.1371%2Fjournal.pone.0037062#pone.0037062Kangas1

[32] M. Kangas, A. Konttila, P. Lindgren, I. Winblad, and T. Jamsa (2008, Feb.). Comparison of low-complexity fall detection algorithms for body attached accelerometers. *Gait and Posture*. [Online]. *28(2)*. 285–291. Available: http://www.gaitposture.com/article/S0966-6362(08)00026-X/abstract

[33] A. C. Guyton, *Textbook of medical physiology*, 7th ed., Saunders, Philadelphia, 1986.

[34] S. Ahmed, N. E. Mayo, J. Higgins, N. M. Salbach, L. Finch, and S. L. Wood, "The stroke rehabilitation assessment of movement: a comparison with other measures used to evaluate effects of stroke and rehabilitation," *J. Physical Therapy*, vol. 83, no. 7, pp. 617–630, July, 2003.

[35] Z. Zhang, Q. Fang, and F. Ferry, "Upper limb motion capturing and classification for unsupervised stroke rehabilitation," in *Proc. IEEE Ind. Electron. Soc. Conf*., Melbourne, Australia, 2011, pp. 3832–3836.

[36] A. S. Anna, A. Salarian, and N. Wickstrom, "A new measure of movement symmentry in early Parkinson's disease patients using symbolic processing of inertial sensor data," *IEEE Trans. Biomedical Eng.*, vol. 58, no. 7, pp. 2127–2136, July, 2011.

[37] S. Ancoli-Israel, R. Cole, C. Alessi, M. Chambers, W. Moorcroft, and C. P. Pollak, "The role of actigraphy in the study of sleep and circadian rhythms," *Sleep*, vol. 26, no. 3, pp. 342–392, 2003.

[38] Philips Respironics, "Actiwatch technical brochure", Available online, http://www.healthcare.philips.com/pwc_hc/au_en/homehealth/actiwatch/pdf/Tie%20as%20Easy%20brochure%20final.pdf, downloaded on 8th May 2012.

[39] CamNtech, "MotionWatch 8 technical brochure", Available online, http://www.camntech.com/images/products/MotionWatch/motionwatch8.pdf, downloaded on 8th May 2012.

[40] Cambridge Neuotechnology Ltd., "Actiwatch Light technical brochure", Available online, http://www.salusa.se/Filer/Produktinfo/Aktivitet/actiwatch light.pdf, downloaded on 8th May 2012.

[41] S. W. Gorny and J. R. Spiro, "Comparing different methodologies used in wrist actigraphy," *Sleep*, pp. 40–42, 2001.

[42] P. J. Hauri and J. Wisbey, "Wrist actigraphy in insomnia," *Sleep*, vol. 15, no. 4, pp. 293–301, 1992.

[43] E. O. Doebelin, *Measurement Systems: application and design*, 4th ed., McGraw-Hill, Singapore, 1990, pp. 320–324.

[44] D. V. S. Murthy, *Transducers and Instrumentation*, Prentice-Hall, India, 1995, pp. 286–292.

[45] M. K. Ghosh, S. Sen, and S. Mukhopadhyay, *Measurements and Instrumentation*, Ane Books, India, 2008, pp. 259–260.

[46] J. W. Dally, W. F. Riley, K. G. McConnell, *Instrumentation for Engineering Measurements*, 2th ed., John Wiely and Sons Pte. Ltd., Singapore, 2006, pp. 320–323.

[47] Freescale semiconductors, "Triaxis Low-g micromachined accelerometer, MMA7331LC", Available online, http://cache.freescale.com/files/sensors/doc/data_sheet/MMA7331LC.pdf?pspll=1, downloaded on 26th May 2011.

[48] Bosh, "Digital triaxial acceleration sensor, BMA180", Available online, http://www.bosch-sensortec.com/content/language1/downloads/BST-BMA180-FL000-03.pdf, downloaded on 20th June 2011.

[49] Freescale Semiconductors, "3-axis, 14-bit/8-bit digital accelerometer, MMA8451Q", Available online, http://cache.freescale.com/files/sensors/doc/data_sheet/MMA8451Q.pdf, downloaded on 20th June 2011.

[50] STMicroelectronics, “MEMS inertial sensor, LIS3LV02DQ”, Available online, http://www.sparkfun.com/datasheets/IC/LIS3LV02DQ.pdf, downloaded on 20th June 2011.

[51] STMicroelectronics, “MEMS motion sensor: ultra-stable three-axis digital output gyroscope, L3G4200D”, Available online, http://www.st.com/internet /com/TECHNICAL_RESOURCES/TECHNICAL_LITERATURE/DATASHE ET/CD00265057.pdf, downloaded on 20th June 2011.

[52] InvenSense, “Motion processing unit product specification rev 1.3, IMU-3000”, Available online, http://invensense.com/mems/gyro/documents/PS-IMU-3000A.pdf, downloaded on 20th June 2011.

[53] Analog Devices, “High performance digital output gyroscope, ADXRS450”, Available online, http://www.analog.com/static/imported-files/data_sheets/ ADXRS450.pdf?r ef=AS C- PR-342, downloaded on 20th June 2011.

[54] D. Ren, L. Wu, M. Yan, M. Cui, Z. You, and M. Hu, “Design and analysis of a MEMS based resonant magnetometer,” in *Proc. IEEE Sensors Conf.*, Christchurch, New Zealand, 2009, pp. 6951–6966.

[55] M. J. Thompson and D. A. Horsley, “Resonant MEMS magnetometer with capacitive read-out,” in *Proc. IEEE Sensors Conf.*, Christchurch, New Zealand, 2009, pp. 992–995.

[56] Honeywell, “3-axis compass with algorithms, HMC6343”, Available online, http://www.honeywell.com/sites/servlet/com.merx.npoint.servlets.DocumentSer vlet?docid=DB8BAEA9F-DB1F-45FF-843E-2F15B0A19786, downloaded on 20th June 2011.

[57] Omni Instruments, “MEMS sensor $MAG^3$, MAG020150S050”, Available online, http://www.omniinstruments.co.uk//images/downloads/2756.pdf, downloaded on 20th June 2011.

[58] Analog Devices, “Tri-axis inertial sensor with magnetometer, ADIS16405”, Available online, http://www.analog.com/static/importedfiles/data_sheets/ ADIS16405.pdf, downloaded on 20th June 2011.

[59] H. Rehbinder and X. Hu, “Drift-free attitude estimation for accelerated rigid bodies,” in *Proc. IEEE Int. Conf. Robot. Autom.*, Seoul, Korea, May 2001, pp. 4244–4249.

[60] E. Kraft, "A quaternion-based unscented Kalman filter for orientation tracking," in *Proc. IEEE 6th Int. Conf. Inf. Fusion*, Cairns, Queensland, Australia, 2003, pp. 47–54.

[61] J. P. How, "Inertial sensors, complementary filtering, and simple Kalman filtering," lecture notes for 16.333, Department of Aeronautics and Astronautics, Massachusetts Institute of Technology, Fall 2004, [Online] Available : http://ocw.mit.edu/courses/aeronautics-and-astronautics/16-333-aircraftstability-and-control-fall-2004/lecture-notes/lecture_15.pdf

[62] C. Verplaetse, "Inertial proprioceptive devices: Self-motion-sensing toys and tools," *IBM Syst.*, vol. 35, no. 3/4, pp. 639–650, 1996.

[63] Microchip Technology, "PIC24FJ64GB004 family data sheet", Available online, http://ww1.microchip.com/downloads/en/DeviceDoc/39940d.pdf, downloaded on 20th June 2011.

[64] Microchip Technology, "64-Mbit SPI serial dual I/O flash, SST25VF064C", Available online, http://ww1.microchip.com/downloads/en/DeviceDoc/25036A.pdf, downloaded on 20th June 2011.

[65] Sipex, "True +3.0V to +5.5V RS-232 transceivers, SP3232E", Available online, http://www.electrojoystick.com/specs/sp3222_3232e.pdf, downloaded on 20th June 2011.

[66] National Semiconductor, "LM1117/LM1117I 800mA low-dropout linear regulator", Available online, http://www.ti.com/lit/ds/symlink/lm1117-n.pdf, downloaded on 20th June 2011.

[67] Educational Control Products, "Model 750Control Moment Gyroscope", Available online, http://www.ecpsystems.com/docs/ECP_Gyroscope_Model_750.pdf, downloaded on 12th June 2012.

[68] E. R. Bachmann, "Inertial and magnetic tracking of limb segment orientation for inserting humans into synthetic environments," Ph.D. dissertation, Naval Postgraduate School, Monterey, CA, 2000.

[69] H. Goldstein, C. Poole, and J. Safko , Classical Mechanics, 3rd ed. Reading, MA: Addison-Wesley , 2002.

[70] J. B. Kuipers, Quaternions and Rotation Sequences. Princeton, NJ: Princeton Univ. Press, 1999.

[71] J. S. Wang, Y. L. Hsu, and J. N. Liu, “An inertial-measurementunit based pen with a trajectory reconstruction algorithm and its applications,” *IEEE Trans. Industrial Electron.*., vol. 57, no. 10, pp. 3508–3521, Oct., 2010.

# Acknowledgements

I express my sincere gratitude towards my guide, Prof. P. C. Pandey for his expert guidance in all the aspects of the project. I want to thank Mr. Nandakumar Pai for all the valuable time, help, suggestions and support he gave me in the project. I would also like to express my sincere thanks to my lab mates in Electronic Instrumentation Lab and Signal Processing and Instrumentation Lab, for their help, and support. I am also thankful to all my friends at IIT for making these last two years unforgettable.

V. Adithya

# Author's resume

**V. Adithya** received the B.E. degree in biomedical engineering from Sri Sivasubramaniya Nadar College of Engineering, Anna University, Chennai, Tamil Nadu in 2010. Presently, she is pursuing the M.Tech. degree in biomedical engineering at the Indian Institute of Technology Bombay. Her research interests include biomedical instrumentation, signal processing and biomechanics.